



Journal Name

ARTICLE

Ligand and solvent control of selectivity in the C-H activation of a pyridylimine-substituted 1-naphthalene; a combined synthetic and computational study

Received 00th January 20xx,
Accepted 00th January 20xx

DOI: 10.1039/x0xx00000x

www.rsc.org/

Abstract: The pyridylimine-substituted 1-naphthalenes, 2-(1-C₁₀H₇)-6-{CR=N(2,6-i-Pr₂C₆H₃)C₅H₃N (R = Me HL_{Me}, H HL_H), react with Na₂[PdCl₄] in acetic acid at elevated temperature to afford either *ortho*-C-H activated (L_{Me})PdCl (2_{ortho}) or the unactivated adduct (HL_H)PdCl₂ (1b). Alternatively, 1b and its ketimine analogue (HL_{Me})PdCl₂ (1a), can be prepared by treating (MeCN)₂PdCl₂ with either HL_{Me} or HL_H in chloroform at room temperature. Regio-selective *ortho*-C-H activation to form 2_{ortho} can also be initiated by the thermolysis of 1a in acetic acid, while no reaction occurs under similar conditions with 1b. Interestingly, the C-H activation of HL_{Me} to give 2_{ortho} is found to be reversible with 100% deuteration of the *peri*-site occurring on reacting Na₂[PdCl₄] with HL_{Me} in acetic acid-d₄. By contrast, heating 1a in toluene gives a 55:45 mixture of 2_{ortho} and its *peri*-activated isomer 2_{peri}. Pure 2_{peri} can, however, be obtained either from (L_{Me})PdOAc (3_{peri}) by OAc/Cl exchange or by the sequential reactions of 1a with firstly silver acetate then with aqueous sodium chloride. Intriguingly, a *peri* to *ortho* interconversion occurs on heating 2_{peri} in acetic acid to give 2_{ortho}. DFT calculations have been used to investigate the C-H activation steps and it is found that in acetic acid *ortho*-C-H activation is kinetically and thermodynamically favoured but *peri*-CH activation is kinetically accessible ($\Delta\Delta G^\ddagger = 2.4 \text{ kcal mol}^{-1}$). By contrast in toluene, the reaction appears to be irreversible with the difference in barrier height for *ortho*- and *peri*-C-H activation very small within error of the method ($\Delta\Delta G^\ddagger = 0.7 \text{ kcal mol}^{-1}$), findings that are agreement with the empirically observed product distribution for 2_{ortho} and 2_{peri}. Single crystal X-ray structures are reported for 1a, 1b, 2_{ortho} and 2_{peri}.

Introduction

Over the past decade a number of highly efficient synthetic strategies have been developed that involve the use of transition metal catalysts to directly cleave non-acidic C-H bonds, a process known as C-H activation.¹⁻⁴ Indeed, these reactions are revolutionizing organic synthesis because they can introduce a more atom economical first step in C-C and C-heteroatom bond forming processes, resulting in a more direct approach to the target transformation.⁵ However, despite the recent significant developments in the field of C-H functionalization, the control of site-selectivity remains a major challenge. Most commonly, a chelating directing group is employed to affect activation of a proximal C-H bond, typically at the *ortho*-site of an aromatic ring.⁶

Recently, metal ligating directing groups have been developed for the alternative activation of remote C-H bonds, including at the *meta*- and *para*-sites of an aromatic ring.⁷ Other factors have also been identified for the control of site-selectivity, including the innate reactivity of the substrate,⁸ the catalyst or metal-ligand combination⁹ and the solvent.¹⁰

In recent years, we have been exploring the factors that influence site-selectivity in the C-H activation of a range of 1-substituted naphthalene molecules, in which we envisaged potential for both *ortho*- and *peri*-C-H activation.¹¹ For example, reaction of the pyridylimine-containing 1-substituted naphthalene, 2-(1-C₁₀H₇)-6-{CMe=N(2,6-i-Pr₂C₆H₃)C₅H₃N (HL_{Me}), with Pd(OAc)₂ led exclusively to *peri*-C-H activation of the naphthyl group, while for the pyridyl-alcohol analogue 2-(1-C₁₀H₇)-6-(CMe₂OH)C₅H₃N solely the *ortho*-C-H activation product was observed (Scheme 1). DFT calculations were performed on the *peri*-pathway which revealed: (i) that the reaction proceeded by a mechanism commonly referred to as a concerted metalation deprotonation (CMD) or ambiphilic metal-ligand activation (AMLA), involving an acetate ligand as an intramolecular base;¹² (ii) that the *peri*-C-H activation was both kinetically and thermodynamically favoured; and (iii) that the site-selectivity of the C-H activation was controlled, in some measure, by the N,N-

^a Department of Chemistry, University of Leicester, University Road, Leicester LE1 7RH, UK.

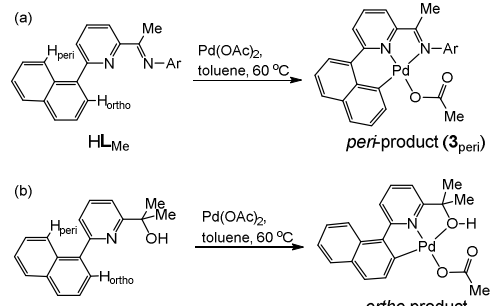
^b School of Science and Technology, Nottingham Trent University, Clifton Lane, Nottingham NG11 8NS, UK

*Corresponding authors: gas8@leicester.ac.uk; warren.cross@ntu.ac.uk
Electronic Supplementary Information (ESI) available: Figures, tables, NMR spectra, computed Cartesian coordinates and energies, details of investigations into other reaction mechanisms. CCDC reference numbers 1586954-1586957. For ESI and crystallographic data in CIF or other electronic format see DOI:

ARTICLE

Journal Name

bidentate directing group, since monodentate directing groups have a preference for the *ortho*-product.¹³⁻¹⁵ Indeed, the formation of the *ortho*-product (Scheme 1b) can be accounted for by assuming the pyridine unit acts as monodentate directing ligand (*c.f.* *ortho*-palladation of 2-(1-naphthyl)pyridine¹⁶), with the OH group coordinating during the final stages of the transformation.



Scheme 1. Acetate-assisted C-H_{naphthyl} activation leading to (a) *peri*- and (b) *ortho*-products; Ar = 2,6-diisopropylphenyl

Given this subtle balance between *ortho*- and *peri*-activation of a naphthalene ring, we decided to explore the reactivity of HL_{Me} and its aldimine analogue, 2-(1-C₁₀H₇)-6-{CH=N(2,6-*i*-Pr₂C₆H₃)}C₅H₃N (HL_H), towards acetate-free palladium(II) sources and in particular the palladium(II) chlorides, (MeCN)₂PdCl₂ and Na₂[PdCl₄]. In these cases, the intramolecular base is now a chloride ligand rather than an κ^1 -acetate and as such a conventional CMD (or AMLA-6) type mechanism will be prevented.¹²

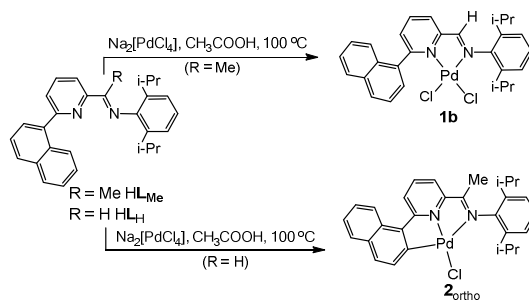
Full details of our synthetic investigation are disclosed with all key intermediates fully characterised. In addition, DFT calculations have been used to support the synthetic findings with a focus on determining the mechanism of C-H activation and the role of the chloride ligand and solvent on the selectivity of these reactions.

Results and discussion

(a) Synthesis and characterization

In the first instance we explored the reactivity of the tetrachloropalladate salt Na₂[PdCl₄] towards HL_{Me} and HL_H. Typically, the reactions were performed in acetic acid at 100 °C over extended reaction times. Using HL_H, precipitation of the adduct (HL_H)PdCl₂ (**1b**) occurred after 24 hours while for HL_{Me}, the C-H activation product (L_{Me})PdCl (**2**_{ortho}) could be isolated in 85% yield after 48–60 hours (Scheme 2). Both **1b** and **2**_{ortho} have been characterized by ¹H/¹³C NMR and IR spectroscopy and mass spectrometry. In addition, both have been the subject of single crystal X-ray diffraction studies.

In the IR spectrum for **1b** the v(C=N)_{imine} band is shifted by *ca.* 30 cm⁻¹ to lower wavenumber compared to free HL_H and consistent with effective coordination with the palladium centre. In the ¹H NMR spectrum thirteen aromatic protons are evident indicating that no C-H activation has occurred; a singlet resonance at δ 8.28 can also be assigned to CH=N proton. In the aliphatic region two



Scheme 2. Synthetic routes to **1b** and **2**_{ortho}

distinct septets and four doublets are seen for the isopropyl protons consistent with both restricted rotation about the Ar-CHMe₂ bond and the inequivalent environment imposed on each isopropyl groups by the positioning of the pendant naphthyl ring above or below the chelate ring. By contrast, in the ¹H NMR spectrum of **2**_{ortho}, only 12 protons in the aromatic region could be detected confirming that C-H activation on the naphthyl moiety has been achieved. With the naphthyl group now coordinated to the palladium, the signals in the aliphatic region show a simpler pattern than in **1b** with the two CH(Me)₂ protons now taking the form of one septet while the CH(Me)₂ protons are seen as only two doublets.

Single crystals of **1b** and **2**_{ortho} were grown by slow diffusion of hexane into dichloromethane solutions containing the respective complex. The structures of **1b** and **2**_{ortho} are different and will be discussed separately. A view of **1b** is given in Figure 1; selected bond distances and angles are listed in Table 1. The structure consists of a palladium centre surrounded by two nitrogen donors belonging to the *N,N*-chelating pyridylimine and two monodentate chloride ligands to complete a distorted square planar geometry. The N(1)-Pd(1)-N(2) bite angle is 79.4(3)[°] which highlights the strain imposed on the geometry by the bidentate ligand. The two Pd-N distances show some variation with the one involving the pyridine longer than that to the imine [Pd(1)-N(1) 2.088(6) vs. Pd(1)-N(2) 2.006(7) Å]. The plane of the naphthyl ring is inclined at 49.1[°] with respect to the neighbouring pyridine ring while the N-2,6-diisopropylphenyl ring is close to perpendicular. The C(7)-N(2) distance of 1.275(9) Å falls in the range typical for an imine group. Related pyridyl-imine-palladium(II) chloride structures have been reported previously and indeed **1b** shows similar features.¹⁷

A perspective view of **2**_{ortho} is shown in Figure 2; selected bond distances and angles are presented in Table 2. In this structure the palladium centre is bound by a tridentate *N,N,C* ligand and a single chloride ligand to form a geometry best described as distorted square planar. The *N,N,C* ligand makes use of the nitrogen donors from the pyridyl and imine units as well as a carbon derived from an *ortho*-activated naphthyl moiety. Two essentially planar five-membered chelate rings are formed with the metal centre with the exterior C-Pd distance notably shorter than the *trans* N_{imine}-Pd distance [Pd(1)-C(15) 1.960(7) vs. Pd(1)-N(1) 2.123(5) Å], likely reflecting the anionic nature of the former and the *trans* influence exerted by the naphthyl group on the imine.

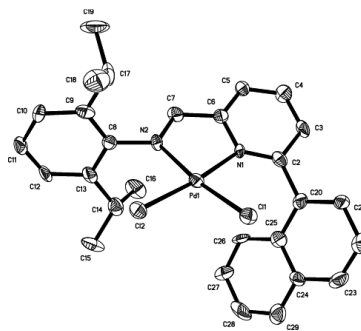


Figure 1. ORTEP representation of **1b** with the thermal ellipsoids set at 50% probability level; all hydrogen atoms are omitted for clarity.

Table 1. Selected bond distances (\AA) and angles ($^\circ$) for **1b**

Pd(1)-N(1)	2.088(6)
Pd(1)-N(2)	2.006(7)
Pd(1)-Cl(1)	2.292(2)
Pd(1)-Cl(2)	2.266(2)
C(7)-N(2)	1.275(9)
C(2)-C(20)	1.502(11)
N(1)-Pd(1)-Cl(1)	99.0(2)
N(1)-Pd(1)-Cl(2)	172.4(2)
N(1)-Pd(1)-N(2)	79.4(3)
N(2)-Pd(1)-Cl(1)	169.8(2)
N(2)-Pd(1)-Cl(2)	93.1(2)
Cl(1)-Pd(1)-Cl(2)	88.57(9)
C(7)-N(2)-C(8)	118.8(8)

In contrast to **1b**, the palladium-nitrogen distance involving the central pyridine is now notably shorter than that to the imine [Pd(1)-N(2) 1.954(5) vs. Pd(1)-N(1) 2.123(5) \AA], an observation presumably attributable to the constraints imposed by the tridentate ligand. The *N*-2,6-diisopropylphenyl group adopts an orientation almost perpendicular to the imine vector (tors.: C(7)-N(1)-C(1)-C(2) 81.1 $^\circ$), while the C-N distance for the imine [1.283(7) \AA] is typical of this functional group. On comparison with the three previously reported examples of crystallographically characterised *ortho*-palladated aryl-substituted pyridylimines, **2_{ortho}** displays comparable features.^{12,18}

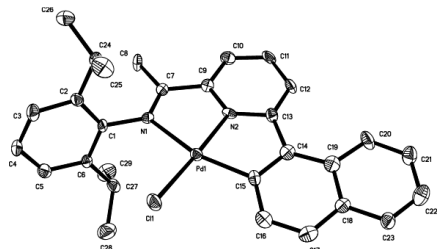


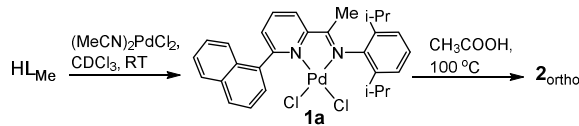
Figure 2. ORTEP representation of **2_{ortho}** with thermal ellipsoids set at 50% probability level; all hydrogen atoms are omitted for clarity.

Table 2. Selected bond lengths (\AA) and angles ($^\circ$) for **2_{ortho}**

Pd(1)-N(1)	2.123(5)
Pd(1)-N(2)	1.954(5)
Pd(1)-C(15)	1.960(7)
Pd(1)-Cl(1)	2.2976(18)
C(7)-N(1)	1.283(7)
C(13)-C(14)	1.499(9)
N(2)-Pd(1)-C(15)	82.1(3)
N(2)-Pd(1)-N(1)	79.7(2)
C(15)-Pd(1)-Cl(1)	98.6(2)
N(1)-Pd(1)-Cl(1)	99.86(15)
C(7)-N(1)-C(1)	123.4(5)

Accordingly, we treated HL_{Me} with $(\text{MeCN})_2\text{PdCl}_2$ in chloroform at room temperature affording $(\text{HL}_{\text{Me}})\text{PdCl}_2$ (**1a**) in high yield (Scheme 3); **1b** could be prepared similarly.

Complex **1a** has been characterised using the same techniques as that described for **1b** and has been the subject of single crystal X-ray diffraction study (see ESI). Indeed, the structure of **1a** shows similar structural features in the solid state to that for **1b** adopting a distorted square planar geometry based on the *N,N* ligand and two chloride ligands (Figure S1). In solution, the key difference between **1b** and **1a** in the ^1H NMR spectrum are the presence of a 3H singlet for the $\text{CMe}=\text{N}$ protons in **1a** and the absence of a downfield $\text{CH}=\text{N}$ proton.



Scheme 3. Stepwise route to **2_{ortho}** *via* **1a**

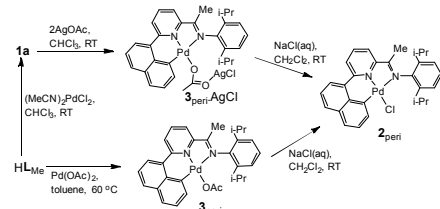
It is assumed that due to the poor solubility of **1b** in hot acetic acid, the subsequent *ortho*-palladation step was impeded. Hence, it would seem probable that a related dichloride species is involved as an intermediate in the formation of **2_{ortho}**, albeit not detectable.

To confirm the role of dichloride complex **1a** as an intermediate in the formation of **2_{ortho}** during the reaction of HL_{Me} with $\text{Na}_2[\text{PdCl}_4]$, we monitored the reaction of **1a** by ^1H NMR spectroscopy which showed the gradual consumption of **1a** and the formation of **2_{ortho}** after 60 hours at 100 °C in acetic acid (Scheme 3), trace amounts (< 5%) of a second product, **2_{peri}** (*vide infra*), were also detectable. Needless to say, **1b** due to its poor solubility in acetic acid, proved unreactive under similar reaction conditions.

With a view to targeting **2_{peri}**, the regio-isomer of **2_{ortho}**, we set about developing a viable synthetic route. Hence, treatment of **1a** with two molar equivalents of silver acetate in chloroform gave a complex we tentatively assign as the C-H activation product [$2-(1-\text{C}_{10}\text{H}_6)-6-(\text{CMe}=\text{N}(2,6-i\text{-Pr}_2\text{C}_6\text{H}_3))\text{C}_5\text{H}_3\text{N}] \text{Pd(OAc)}_2\text{AgCl}$ (**3_{peri}·AgCl**), which on further reaction with aqueous sodium chloride gave **2_{peri}** in good yield (Scheme 4). Alternatively, **2_{peri}** could be obtained in comparable yield by a similar acetate-chloride exchange using pure **3_{peri}** previously prepared by the reaction of HL_{Me} with Pd(OAc)_2 in toluene.¹²

ARTICLE

Journal Name

**Scheme 4.** Synthetic routes to $\mathbf{2}_{\text{peri}}$

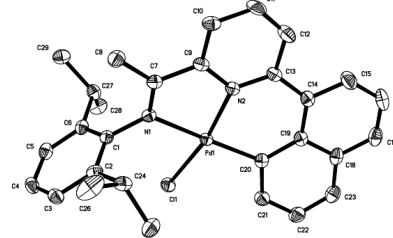
The precise structural identity of intermediate $\mathbf{3}_{\text{peri}}\cdot\text{AgCl}$ remains uncertain but the presence of 12 aromatic protons and only one acetate-Me is consistent with C-H activation having occurred. However, there is some variation of the chemical shift of the signals in the ^1H NMR spectrum in CDCl_3 when compared with $\mathbf{3}_{\text{peri}}$, therefore we have ascribed this to adduct formation having occurred between $\mathbf{3}_{\text{peri}}$ and the AgCl that is eliminated during the reaction.

Complex $\mathbf{2}_{\text{peri}}$ has been characterised spectroscopically and has been subject of a single crystal X-ray diffraction study. Single crystals suitable for the study could be grown by slow diffusion of hexane into a dichloromethane solution of the complex. A perspective view of $\mathbf{2}_{\text{peri}}$ is given in Figure 3; selected bond distances and angles are collected in Table 3. The structure resembles $\mathbf{2}_{\text{ortho}}$ with a distorted square planar palladium centre bound by a N,N,C tridentate ligand along with a monodentate chloride ligand. The key difference in $\mathbf{2}_{\text{peri}}$ is that the naphthyl moiety binds through the *peri*-carbon with the result that it is incorporated into a six-membered chelate ring. The larger ring system has the effect that the $\text{N}_{\text{pyridine}}\text{-Pd-C}_{\text{naphthyl}}$ bite angle of $94.14(11)^\circ$ is more compatible with the geometrical requirements of the square planar geometry [*c.f.* $82.1(3)^\circ$ in $\mathbf{2}_{\text{ortho}}$]. As with $\mathbf{2}_{\text{ortho}}$ there are some consequent variations in the bond lengths between palladium and the donor atoms belonging to the N,N,C ligand with $\text{Pd-N}_{\text{imine}} (2.104(2) \text{\AA}) > \text{Pd-N}_{\text{pyridine}} (2.018(2) \text{\AA}) > \text{Pd-C}_{\text{naphthyl}} (1.987(3) \text{\AA})$. In comparison with $\mathbf{2}_{\text{ortho}}$ the $\text{Pd-C}_{\text{naphthyl}}$ distance is marginally longer in $\mathbf{2}_{\text{peri}}$ [$1.987(3) \text{ vs. } 1.960(7) \text{\AA}$] with the effect that the $\text{Pd-N}_{\text{imine}}$ distance in $\mathbf{2}_{\text{peri}}$ is relatively shorter [$2.104(2)$ ($\mathbf{2}_{\text{peri}}$) *vs.* $2.123(5) \text{\AA}$ ($\mathbf{2}_{\text{ortho}}$)]. The N-aryl ring is again inclined close to perpendicular with respect to the imine vector [tors.: $\text{C}(7)\text{-N}(1)\text{-C}(1)\text{-C}(2) 84.8^\circ$].

In the FAB mass spectrum of $\mathbf{2}_{\text{peri}}$ a molecular ion peak as well as a fragmentation peak corresponding to the loss of a chloride are evident. Like $\mathbf{2}_{\text{ortho}}$ there are two inequivalent CHMe_aMe_b methyl groups at each *ortho*-site which manifests itself as two 6H doublets in the ^1H NMR spectrum. The imine carbon is seen as the most downfield signal at $\delta 171.2$ in the ^{13}C NMR spectrum while the imine methyl is visible as the most upfield signal at $\delta 18.7$.

(b) Mechanistic considerations

In contrast to our previous findings with $\text{Pd}(\text{OAc})_2$,¹² the selective formation of $\mathbf{2}_{\text{ortho}}$ from either the reaction of HL_Me with $\text{Na}_2[\text{PdCl}_4]$ in acetic acid at high temperature or by the thermolysis of $\mathbf{1a}$ in acetic acid raises some intriguing questions. For example, (i) are these transformations reversible, (ii) is the nature of the solvent

**Figure 3.** ORTEP representation of $\mathbf{2}_{\text{peri}}$ with the thermal ellipsoids set at 50% probability level; all hydrogen atoms are omitted for clarity.**Table 3.** Selected bond lengths (\AA) and angles ($^\circ$) for $\mathbf{2}_{\text{peri}}$

Pd(1)-N(1)	2.104(2)
Pd(1)-N(2)	2.018(2)
Pd(1)-C(20)	1.987(3)
Pd(1)-Cl(1)	2.3259(8)
C(7)-N(1)	1.282(3)
C(13)-C(14)	1.497(4)
N(2)-Pd(1)-C(20)	94.14(11)
N(2)-Pd(1)-N(1)	80.68(9)
C(20)-Pd(1)-Cl(1)	95.02(9)
N(1)-Pd(1)-Cl(1)	90.87(6)
C(7)-N(1)-C(1)	121.4(2)

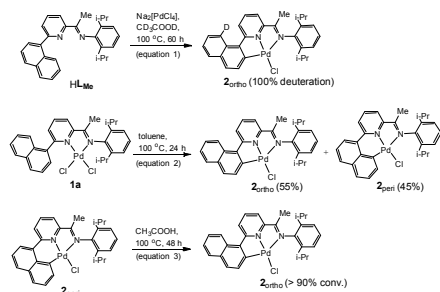
important on the selectivity and (iii) does $\mathbf{2}_{\text{peri}}$ convert to $\mathbf{2}_{\text{ortho}}$ in acetic acid at high temperature?

To explore the reversibility of the C-H activation, we carried out a small scale reaction of HL_Me with $\text{Na}_2[\text{PdCl}_4]$ in acetic acid- d_4 at 100°C (Scheme 5, equation 1). Inspection of the ^1H NMR spectrum revealed the formation of $\mathbf{2}_{\text{ortho}}$ in which 100% deuteration at the *peri*-position had occurred (the corresponding protio-signal had disappeared, see SI). Therefore, this finding would suggest that this palladation reaction in acetic acid is reversible.

With a view to probing the role played by solvent on the selectivity of the C-H activation, we explored the thermolysis of $\mathbf{1a}$ in toluene, initially at 60°C for 12 hours. At this temperature the reaction was incomplete, with 70% starting material still present but with the remaining 30% comprised of an approximately equal mixture of $\mathbf{2}_{\text{ortho}}$ and $\mathbf{2}_{\text{peri}}$. However, on raising the temperature to 100°C , full consumption of starting material was noted and the formation of a 55:45 mixture of $\mathbf{2}_{\text{ortho}}$ and $\mathbf{2}_{\text{peri}}$ was observable after 24 hours (Scheme 5, equation 2). Hence, it would seem apparent that the high selectivity for $\mathbf{2}_{\text{ortho}}$ observed in acetic acid is affected by the choice of solvent.

Given the preference for $\mathbf{2}_{\text{ortho}}$ when the C-H activation reactions were performed in acetic acid, it was of interest to establish if the isomer $\mathbf{2}_{\text{peri}}$ would undergo conversion to $\mathbf{2}_{\text{ortho}}$ on heating in acetic acid. Hence, monitoring a reaction of pure $\mathbf{2}_{\text{peri}}$ at 100°C in acetic acid revealed that after 60 hours greater than 90% conversion to $\mathbf{2}_{\text{ortho}}$ was achieved (Scheme 5, equation 3). Likewise, taking the 55:45 mixture of $\mathbf{2}_{\text{ortho}}$ and $\mathbf{2}_{\text{peri}}$ that was obtained from the reaction in toluene, and heating it in acetic acid at 100°C

resulted in similar conversion to **2_{ortho}**. This corroborates both the selectivity for *ortho*-C–H activation and the reversibility of the reaction in acetic acid.



Scheme 5. Experiments exploring reversibility, solvent and interconversion chemistry; conversions and ratios (%) determined using ^1H NMR spectroscopy (in CDCl_3)

(c) Computational studies

Density functional theory (DFT) calculations were employed to further investigate the site-selectivity for the reaction of pyridyl-naphthalene **HL_{Me}** with $\text{Na}_2[\text{PdCl}_4]$. The energies discussed in the main text are Gibbs energies that include both a dispersion correction and a solvent correction (AcOH or toluene).

First, we computed the structures of the two isomeric products **2_{ortho}** and **2_{peri}**. The optimised structures are in accord with the solid-state structures obtained from single crystal X-ray diffraction. The computed solution energy of the *ortho*-isomer **2_{ortho}** was 1.2 $\text{kcal}\cdot\text{mol}^{-1}$ lower than that of the *peri*-isomer **2_{peri}** in acetic acid and 1.4 $\text{kcal}\cdot\text{mol}^{-1}$ lower in toluene. This difference in energies is consistent with the *ortho*-isomer **2_{ortho}** being the thermodynamic product of the C–H activation reaction.

Next, we investigated the kinetic barriers to the alternative *ortho*- and *peri*-C–H activations of the PdCl_2 complex **1a**. Whereas C–H activation mediated by palladium carboxylate complexes has been thoroughly investigated by computational methods,¹² C–H activation by palladium chloride complexes has been less well studied.¹⁹ We have ruled out an acetic acid mediated LPdCl_2 to LPd(OAc)_2 transformation as (i) such conversions rely on salt elimination approaches, and (ii) if an acetate ligand was generated it would drive a *peri*-selectivity. Therefore, a number of plausible reaction mechanisms were investigated based on dichloride **1a**, including oxidative addition and concerted metalation-deprotonation (CMD or ambiphilic metal ligand activation, AMLA); for the CMD reaction, mechanisms involving both inner- and outer-sphere chloride were studied. The inner-sphere CMD mechanism, as shown in Figure 4, proved to be the lowest energy pathway for both the *ortho*- and *peri*-C–H activation of **1a** (see ESI for a comparison of all the mechanisms investigated).

For the *ortho*-C–H activation of **1a**, a one-step reaction was found, involving the direct cleavage of the *ortho*-C–H bond and concomitant transfer of the H atom to the nearest chloride ligand (Figure 4). In contrast with the commonly observed CMD mechanism involving a metal κ^1 -acetate, which has a 6-membered ring transition state, this reaction involving a palladium chloride has

a 4-membered ring transition state. This CMD reaction proceeds *via* TS(**1a**–**B_{ortho}**) ($\Delta G^\ddagger(\text{AcOH}) = 20.4 \text{ kcal}\cdot\text{mol}^{-1}$; $\Delta G^\ddagger(\text{PhMe}) = 21.3 \text{ kcal}\cdot\text{mol}^{-1}$) to give the intermediate HCl complex **B_{ortho}** ($\Delta G(\text{AcOH}) = 6.5 \text{ kcal}\cdot\text{mol}^{-1}$; $\Delta G(\text{PhMe}) = 3.9 \text{ kcal}\cdot\text{mol}^{-1}$); subsequent dissociation of HCl gives the product **2_{ortho}** ($\Delta G(\text{AcOH}) = -34.0 \text{ kcal}\cdot\text{mol}^{-1}$; $\Delta G(\text{PhMe}) = -36.0 \text{ kcal}\cdot\text{mol}^{-1}$).

By contrast, for the *peri*-C–H activation of **1a** a two-step reaction was found, involving a change in geometry at the metal prior to C–H cleavage (Figure 4). First, square planar complex **1a** is transformed to intermediate **A** ($\Delta G(\text{AcOH}) = 16.4 \text{ kcal}\cdot\text{mol}^{-1}$; $\Delta G(\text{PhMe}) = 16.3 \text{ kcal}\cdot\text{mol}^{-1}$), *via* TS(**1a**–**A**) ($\Delta G^\ddagger(\text{AcOH}) = 22.8 \text{ kcal}\cdot\text{mol}^{-1}$; $\Delta G^\ddagger(\text{PhMe}) = 22.0 \text{ kcal}\cdot\text{mol}^{-1}$). Intermediate **A** adopts a square-based pyramidal geometry, with an agostic *peri*-C–H interaction displacing the closest chloride ligand, which now occupies the apical site. The subsequent activation of the *peri*-C–H bond in **A** (also *via* a 4-membered ring transition state) is effectively a barrierless reaction: once the dispersion and solvent corrections have been applied to the gas phase free energy, the transition state TS(**A**–**B_{peri}**) is lower in energy than intermediate **A** ($\Delta G^\ddagger(\text{AcOH}) = 15.7 \text{ kcal}\cdot\text{mol}^{-1}$; $\Delta G^\ddagger(\text{PhMe}) = 16.2 \text{ kcal}\cdot\text{mol}^{-1}$). The two transition states, TS(**1a**–**A**) and TS(**A**–**B_{peri}**), are similar in structure; the major difference is a shorter Pd–Cl distance in TS(**1a**–**A**), and a shorter Pd–C···H distance in TS(**A**–**B_{peri}**). Importantly, the first transition state, TS(**1a**–**A**), is the highest energy point on the *peri*-C–H activation pathway. The direct product of the *peri*-C–H activation is also an HCl adduct, **B_{peri}** ($\Delta G(\text{AcOH}) = 7.7 \text{ kcal}\cdot\text{mol}^{-1}$; $\Delta G(\text{PhMe}) = 5.2 \text{ kcal}\cdot\text{mol}^{-1}$); as with **B_{ortho}** dissociation of HCl then gives the product **2_{peri}** ($\Delta G(\text{AcOH}) = -32.8 \text{ kcal}\cdot\text{mol}^{-1}$; $\Delta G(\text{PhMe}) = -34.6 \text{ kcal}\cdot\text{mol}^{-1}$).

Considering the reaction in acetic acid first: the computed *ortho*-C–H activation reaction is both thermodynamically favoured ($\Delta G(\text{AcOH}) = 1.2 \text{ kcal}\cdot\text{mol}^{-1}$) and kinetically favoured ($\Delta \Delta G^\ddagger = 2.4 \text{ kcal}\cdot\text{mol}^{-1}$). Importantly, with this small difference in free-energy barrier heights, the *peri*-C–H activation reaction pathway is still kinetically accessible. If the reaction in AcOH is reversible, which the experimental findings suggest, then these computational findings are consistent with the observation that the reaction in acetic acid- d_4 produces only **2_{ortho}**, yet the *peri*-site undergoes 100% deuteration. We suggest that the abundant source of protons available in acetic acid renders the reaction readily reversible. However, given the large barrier for the reverse of this computed reaction, the mechanism for this equilibration is unknown.

Considering the reaction in toluene next: the computed *ortho*-C–H activation reaction is still thermodynamically favoured ($\Delta G(\text{PhMe}) = 1.4 \text{ kcal}\cdot\text{mol}^{-1}$), but now the difference in free-energy barrier heights is very small ($\Delta \Delta G^\ddagger = 0.7 \text{ kcal}\cdot\text{mol}^{-1}$). If the reaction in toluene is irreversible, the calculated product distribution ($2_{\text{ortho}}/2_{\text{peri}} = 72:28$ at 100 °C) is similar to the experimental observation ($2_{\text{ortho}}/2_{\text{peri}} = 55:45$); indeed, the difference in barrier heights that corresponds to these different product distributions (0.55 $\text{kcal}\cdot\text{mol}^{-1}$) is within the error of the computational method.²⁰ We again suggest that the lack of an abundant proton source in toluene renders the reaction effectively irreversible.



Journal Name

ARTICLE

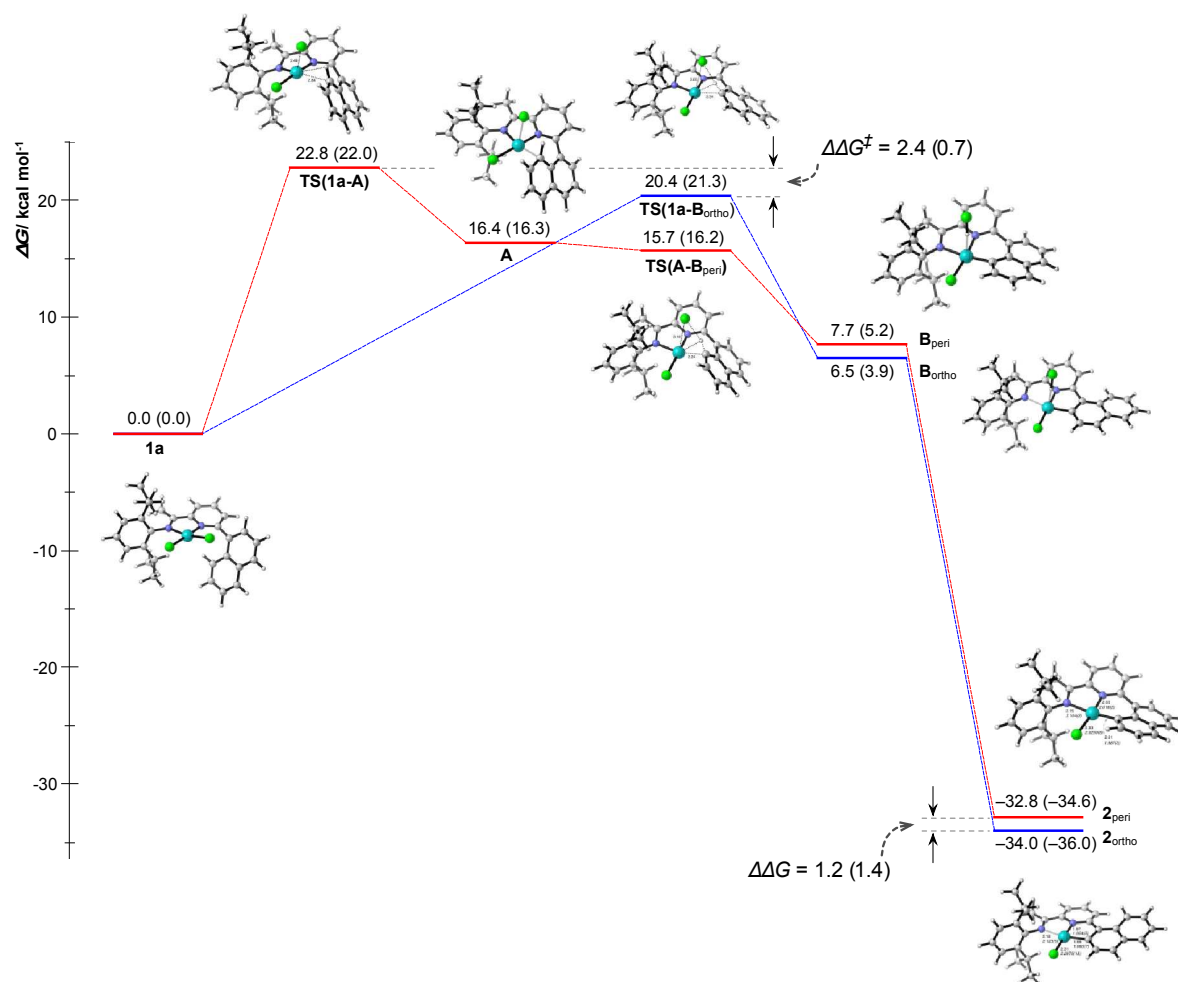


Figure 4. Computed reaction profile for the C-H activation of **1a** via an inner-sphere concerted-metallation-deprotonation mechanism. Energies were calculated at the BP86-D3/SDD/6-31G(d,p) level and include a PCM solvent correction; energies are presented for both acetic acid and toluene (parentheses).

This computational investigation highlights several factors that have the potential to influence the selectivity of C-H activation: (i) the effect of the solvent on the relative energies of products, intermediates and transition states; (ii) whether the conditions of the reaction render it reversible or not; and (iii) the reaction pathways involved. In this study, the transition state for C-H cleavage is always lower for the *peri*-C-H activation, TS(**A**-B_{peri}) vs. TS(**1a**-B_{ortho}). However, since the *peri*-C-H activation is a two-step

reaction that has a higher energy transition state TS(**1a**-A) prior to C-H cleavage, the one-step *ortho*-C-H activation is either kinetically favoured (in AcOH), or has an almost identical activation energy (in PhMe).

Conclusions

C-H activation of HL_{Me} with $\text{Na}_2[\text{PdCl}_4]$ in acetic acid at elevated temperature occurs selectively at the *ortho*-position of the naphthyl ring to give **2**_{ortho}. The dichloride intermediate **1a** has been isolated

and shown to convert to **2_{ortho}** under similar reaction conditions. DFT calculations have shown that in acetic acid *ortho*-C-H activation is kinetically and thermodynamically favoured but *peri*-C-H activation is kinetically accessible ($\Delta\Delta G^\ddagger = 2.4 \text{ kcal mol}^{-1}$). Indeed, *peri*-deuteration of **2_{ortho}** has been achieved on reaction of **HL_{Me}** with Na₂[PdCl₄] in acetic acid-*d*₄. In addition, conversion of **2_{peri}** to **2_{ortho}** has been shown to occur in acetic acid at high temperature. In contrast, in toluene the reaction is found to be irreversible with the difference in barrier height for *ortho*- and *peri*-C-H activation very small ($\Delta\Delta G^\ddagger = 0.7 \text{ kcal mol}^{-1}$), a finding that is supported by the observed product distribution for **2_{ortho}** and **2_{peri}** on heating **1a** in toluene. Overall, this investigation highlights the potential for a number of factors to influence the selectivity of C-H activation, including the reaction pathway, the solvent, and, for a CMD or AMLA reaction, the ligand functioning as an intramolecular base. We view these findings are of significant relevance in the pursuit of new methods for site-selectivity in catalytic C-H functionalization.

Experimental Section

General

All operations, unless otherwise stated, were carried out in vessels open to the air and reagent grade solvents used in each case. The electrospray (ESI) mass spectra were recorded using a micromass Quattro LC mass spectrometer with methanol as the matrix. FAB mass spectra (including high resolution) were recorded on Kratos Concept spectrometer with *m*-nitrobenzyl alcohol (NBA) as matrix. The infrared spectra were recorded in the solid state with Universal ATR sampling accessories on a Perkin Elmer Spectrum One FTIR instrument. NMR spectra were recorded on Bruker ARX-400 spectrometer (400 MHz for ¹H, 100 MHz for ¹³C) or a Bruker Avance III 500 spectrometer (500 MHz for ¹H, 125 MHz for ¹³C), at ambient temperature unless otherwise stated; chemical shifts (ppm) are referred to the residual protic solvent peaks and coupling constants are expressed in hertz (Hz). Melting points (mp) were measured on a Gallenkamp melting point apparatus (model MFB-595) in open capillary tubes and were uncorrected. Elemental analyses were performed at the Science Technical Support Unit, London Metropolitan University. The reagents were purchased from Aldrich Chemical Co. and used without further purification. The compounds, 2-(1-C₁₀H₇)-6-{CR=N(2,6-*i*-Pr₂C₆H₃)C₅H₃N (R = Me **HL_{Me}**, H **HL_H**),¹² bis(acetonitrile)dichloropalladium(II)²¹ and *peri*-(**L_{Me}**PdOAc (**3_{peri}**) were prepared using literature procedures.¹²

Reaction of **HL_H** with Na₂[PdCl₄]

To a 50 mL round-bottom flask, equipped with a stir bar open to the air, was added **HL_H** (0.050 g, 0.14 mmol), Na₂[PdCl₄] (0.040 g, 0.14 mmol) and acetic acid (5 mL). A reflux condenser was attached and the mixture stirred and heated to 100 °C for 24 h resulting in the formation of an orange precipitate. Upon cooling to room temperature, the suspension was filtered to give **1b** as an orange powder (0.065 g, 81%). Recrystallization from dichloromethane/hexane gave orange crystals suitable for a single crystal X-ray diffraction study. ¹H NMR (CD₂Cl₂, 500 MHz): δ 1.24 (d, 3H, ³J_{HH} = 6.9 Hz, CH(CH₃)₂), 1.30 (d, 3H, ³J_{HH} = 6.9 Hz, CH(CH₃)₂),

1.44 (d, 3H, ³J_{HH} = 6.8 Hz, CH(CH₃)₂), 1.47 (d, 3H, ³J_{HH} = 6.8 Hz, CH(CH₃)₂), 3.41 (sept, 1H, ³J_{HH} = 6.8 Hz, CH(CH₃)₂), 3.49 (sept, 1H, ³J_{HH} = 6.9 Hz, CH(CH₃)₂), 7.27 (d, 2H, ³J_{HH} = 6.3 Hz, Ar-H), 7.41 (t, 1H, ³J_{HH} = 6.3 Hz, Ar-H), 7.65-7.70 (m, 3H, Ar-H), 7.79 (d, 1H, ³J_{HH} = 5.7 Hz, ³J_{HH} = 1.0 Hz, Ar-H), 7.94-8.02 (m, 3H, Ar/Py-H_m), 8.04 (d, 1H, ³J_{HH} = 6.4 Hz, Ar-H), 8.09 (d, 1H, ³J_{HH} = 6.3 Hz, Py-H_m), 8.28 (m, 2H, Py-H_p, CH=N). ¹³C{¹H} NMR (CD₂Cl₂, 125 MHz): δ 23.2 (Ar-CHMe₂), 23.3 (Ar-CHMe₂), 24.6 (Ar-CHMe₂), 24.7 (Ar-CHMe₂), 29.2 (Ar-CHMe₂), 29.3 (Ar-CHMe₂), 123.8 (CH), 123.9 (CH), 124.8 (CH), 125.4 (CH), 126.7 (CH), 127.4 (CH), 127.5 (CH), 128.8 (C), 129.1 (CH), 129.2 (CH), 130.1 (CH), 131.2 (CH), 132.0 (C), 133.8 (C), 134.2 (CH), 135.1 (C), 137.1 (C), 139.9 (CH), 141.2 (C), 155.2 (C), 155.5 (C), 170.1 (HCMe=N). IR (cm⁻¹): 1585 v(C=N)_{pyridine}, 1626 v(C=N)_{imine}. ESIMS (+ve, MeOH) *m/z*: 498 [M-Cl]⁺. HRMS (FAB): calculated for C₂₈H₂₇N₂Pd [M-HCl]⁺ 497.1209, found 497.1235. Mp: 250-252 °C. Anal. calc. for (C₂₈H₂₈N₂Cl₂Pd_{0.6}CH₂Cl₂): C 55.33, H 4.34, N 4.51. Found C 55.12, H 4.81, N 4.30%.

Reaction of **HL_{Me}** with Na₂[PdCl₄]

To a round-bottom flask, equipped with a stir bar open to the air, was added **HL_{Me}** (0.100 g, 0.25 mmol), Na₂[PdCl₄] (0.074 g, 0.25 mmol) and glacial acetic acid (5 mL). A condenser was attached and the mixture stirred and heated to 100 °C for 60 h. Upon cooling to room temperature, the resulting suspension was filtered to give **2_{ortho}** as an orange powder (0.116 g, 85%). Recrystallization from dichloromethane/hexane yielded orange crystals suitable for a single crystal X-ray diffraction study. ¹H NMR (CDCl₃, 500 MHz): δ 1.16 (d, 6H, ³J_{HH} = 6.9 Hz, CH(CH₃)₂), 1.39 (d, 6H, ³J_{HH} = 6.9 Hz, CH(CH₃)₂), 2.22 (s, 3H, NCCH₃), 3.07 (sept, 2H, ³J_{HH} = 6.9 Hz, CH(CH₃)₂), 7.25 (s, 3H, dipp-H), 7.41 (t, 1H, ³J_{HH} = 7.6 Hz, Ar-H), 7.49-7.54 (m, 2H, Ar/Py-H), 7.60 (d, 1H, ³J_{HH} = 7.8 Hz, Ar-H), 7.84 (d, 1H, ³J_{HH} = 7.6 Hz, Ar-H), 8.02 (t, 1H, ³J_{HH} = 8.0 Hz, Py-H), 8.20 (d, 1H, ³J_{HH} = 8.0 Hz, Ar-H), 8.35 (d, 1H, ³J_{HH} = 7.4 Hz, Ar-H), 8.37 (d, 1H, ³J_{HH} = 8.0 Hz, Py-H). A ¹³C{¹H} NMR spectrum could not be obtained due to the sample's insufficient solubility in CDCl₃ and other common NMR solvents. IR (cm⁻¹): 755 v(C-H bend), 796 v(C-H bend), 1590 v(C-N)_{pyridine}, 1629 v(C=N)_{imine}, 2966 v(C-H stretch). ESIMS (+ve, MeOH): *m/z* 547 [M]⁺. HRMS (FAB): calculated for C₂₉H₂₉N₂PdCl [M]⁺ 547.2023 and C₂₉H₂₉N₂Pd [M-Cl]⁺ 511.1088, found 547.2017 and 511.1079. Mp: > 270 °C. Anal. calc. for (C₂₉H₂₉ClN₂Pd): C 63.63, H 5.34, N 5.12. Found C 63.55, H 5.29, N 5.18%.

Synthesis of (**HL_R**)PdCl₂ (**1a R = Me; 1b R = H**)

(a) R = Me (**1a**). To a 50 mL round-bottom flask, equipped with a stir bar and open to the air, was added **HL_{Me}** (0.100 g, 0.25 mmol), (MeCN)₂PdCl₂ (0.064 g, 0.25 mmol) and chloroform (5 mL). The mixture was then stirred at room temperature for 24 h. The solvent was removed under reduced pressure and the crude product recrystallized from dichloromethane/hexane to give **1a** as an orange powder (0.110 g, 75%). Slow evaporation of a chloroform solution of the product yielded orange crystals suitable for a single crystal X-ray diffraction study. ¹H NMR (CD₂Cl₂, 500 MHz): δ 1.19 (d, 3H, ³J_{HH} = 6.9 Hz, CH(CH₃)₂), 1.23 (d, 3H, ³J_{HH} = 6.8 Hz, CH(CH₃)₂), 1.42 (d, 3H, ³J_{HH} = 6.9 Hz, CH(CH₃)₂), 1.46 (d, 3H, ³J_{HH} = 6.8 Hz, CH(CH₃)₂), 2.31 (s, 3H, NCCH₃), 3.17 (sept, 1H, ³J_{HH} = 6.9 Hz, CH(CH₃)₂), 3.27 (sept, 1H, ³J_{HH} = 6.8 Hz, CH(CH₃)₂), 7.24 (d, 2H, ³J_{HH} = 8.0 Hz, dipp-H), 7.36 (t, 1H, ³J_{HH} = 8.0 Hz, dipp-H), 7.57-7.65 (m, 3H,

ARTICLE

Journal Name

Ar-H), 7.76 (dd, 1H, $^3J_{HH} = 7.6$ Hz, $^3J_{HH} = 1.2$ Hz, Ar-H), 7.91 (m, 1H, Py-H), 7.96–7.99 (m, 3H, Py-H), 8.03 (d, 1H, $^3J_{HH} = 8.2$ Hz, Ar-H), 8.19 (t, 1H, $^3J_{HH} = 7.8$ Hz, Ar-H). $^{13}\text{C}\{\text{H}\}$ NMR (CD_2Cl_2 , 125 MHz): δ 21.1 (CMe=N), 23.8 (Ar-CHMe₂), 23.8 (Ar-CHMe₂), 24.0 (Ar-CHMe₂), 26.6 (Ar-CHMe₂), 29.3 (Ar-CHMe₂), 29.4 (Ar-CHMe₂), 124.0 (CH), 124.1 (CH), 125.0 (CH), 125.4 (CH), 125.8 (CH), 126.6 (CH), 127.5 (CH), 128.8 (CH), 129.2 (CH), 130.1 (CH), 131.0 (CH), 131.9 (C), 133.9 (C), 134.0 (CH), 137.8 (C), 139.8 (CH), 140.4 (C), 140.5 (C), 141.4 (C), 157.0 (C), 164.8 (C), 178.3 (CMe=N). IR (cm^{-1}): 1595 $\nu(\text{C}=\text{N})_{\text{pyridine}}$, 1614 $\nu(\text{C}=\text{N})_{\text{imine}}$, 2956 $\nu(\text{C}-\text{H stretch})$. ESIMS (+ve, MeOH): *m/z* 511 [M-2Cl]⁺. HRMS (FAB): calculated for $\text{C}_{29}\text{H}_{30}\text{N}_2\text{Pd}$ [M-2Cl]⁺ 511.1365, found 511.1382. Mp: 254–256 °C. Anal. calc. for ($\text{C}_{29}\text{H}_{30}\text{N}_2\text{Cl}_2\text{Pd}$ 0.45CHCl₃): C 55.48, H 4.81, N 4.39. Found C 55.60, H 4.75, N 4.82%.

(b) R = H (**1b**). Using a procedure and molar ratios similar to that described for **1a**, **1b** could be isolated as an orange powder (0.112 g, 79%). The spectroscopic and analytical data were as described above.

Conversion of 1a to 2_{ortho}

To a 25 mL round-bottom flask, equipped with a stir bar and open to the air, was added **1a** (0.010 g, 0.018 mmol), AgOAc (0.006 g, 0.036 mmol, 2 eq.) and chloroform (3 mL). The mixture was stirred at room temperature overnight, resulting in a white/grey precipitate. Following filtration, the solvent was removed under reduced pressure to give **3_{peri}·AgCl** as a yellow powder (0.011 g, 87%). ^1H NMR (CDCl_3 , 400 MHz): δ 1.02 (d, 6H, $^3J_{HH} = 6.5$ Hz, CH(CH₃)₂), 1.17 (br s, 3H, Pd-OC(O)CH₃), 1.22 (d, 6H, $^3J_{HH} = 6.5$ Hz, CH(CH₃)₂), 2.32 (s, 3H, (CH₃)C=N), 2.96–3.11 (m, 2H, CH(CH₃)₂), 7.03–7.09 (m, 1H, Ar/Py-H), 7.14–7.16 (m, 2H, Ar/Py-H), 7.19 (s, 2H, Ar/Py-H), 7.50 (t, 1H, $^3J_{HH} = 7.8$ Hz, Ar/Py-H), 7.54 (d, 1H, $^3J_{HH} = 7.9$ Hz, Ar/Py-H), 7.89 (d, 1H, $^3J_{HH} = 7.6$ Hz, Ar/Py-H), 7.95 (d, 1H, $^3J_{HH} = 7.8$ Hz, Ar/Py-H), 8.18–8.23 (m, 2H, Ar/Py-H), 8.47 (d, 1H, $^3J_{HH} = 8.4$ Hz, Ar/Py-H). HRMS (FAB): calculated for $\text{C}_{29}\text{H}_{29}\text{N}_2\text{Pd}$ [M-(OAc-AgCl)]⁺ 511.1365, found 511.1357.

511.1079. Mp: > 270 °C. Anal. calc. for ($\text{C}_{29}\text{H}_{29}\text{N}_2\text{ClPd}$): C 63.63, H 5.34, N 5.12. Found C 63.57, H 5.46, N 5.39%.

Conversion of 1a to 2_{peri} via (3_{peri}·AgCl)

(a) Step 1. To a 25 mL round-bottom flask, equipped with a stir bar and open to the air, was added **1a** (0.010 g, 0.018 mmol), AgOAc (0.006 g, 0.036 mmol, 2 eq.) and chloroform (3 mL). The mixture was stirred at room temperature overnight, resulting in a white/grey precipitate. Following filtration, the solvent was removed under reduced pressure to give **3_{peri}·AgCl** as a yellow powder (0.011 g, 87%). ^1H NMR (CDCl_3 , 400 MHz): δ 1.02 (d, 6H, $^3J_{HH} = 6.5$ Hz, CH(CH₃)₂), 1.17 (br s, 3H, Pd-OC(O)CH₃), 1.22 (d, 6H, $^3J_{HH} = 6.5$ Hz, CH(CH₃)₂), 2.32 (s, 3H, (CH₃)C=N), 2.96–3.11 (m, 2H, CH(CH₃)₂), 7.03–7.09 (m, 1H, Ar/Py-H), 7.14–7.16 (m, 2H, Ar/Py-H), 7.19 (s, 2H, Ar/Py-H), 7.50 (t, 1H, $^3J_{HH} = 7.8$ Hz, Ar/Py-H), 7.54 (d, 1H, $^3J_{HH} = 7.9$ Hz, Ar/Py-H), 7.89 (d, 1H, $^3J_{HH} = 7.6$ Hz, Ar/Py-H), 7.95 (d, 1H, $^3J_{HH} = 7.8$ Hz, Ar/Py-H), 8.18–8.23 (m, 2H, Ar/Py-H), 8.47 (d, 1H, $^3J_{HH} = 8.4$ Hz, Ar/Py-H). HRMS (FAB): calculated for $\text{C}_{29}\text{H}_{29}\text{N}_2\text{Pd}$ [M-(OAc-AgCl)]⁺ 511.1365, found 511.1357.

(b) Step 2: Intermediate **3_{peri}·AgCl** was then dissolved in dichloromethane (5 mL) and stirred vigorously with a saturated aqueous sodium chloride solution at room temperature for 2 h. The organic layer was separated and the aqueous layer washed with dichloromethane (3 x 5 mL). The organic phases were combined, dried over MgSO₄ and the solvent removed under reduced pressure affording **2_{peri}** as a yellow solid (0.007 g, 73%). The spectroscopic and analytical data were as described above.

Peri-deuteration of 2_{ortho}

To a 25 mL round-bottom flask, equipped with a stir bar and open to the air, was added HL_{Me} (0.005 g, 0.012 mmol), Na₂[PdCl₄] (0.004 g, 0.012 mmol) and CD₃COOD (3 mL). A condenser was attached and the mixture stirred and heated to 100 °C for 60 h. Upon cooling to room temperature, the resulting suspension was filtered to give the crude product. Recrystallization from CH₂Cl₂/hexane yielded *peri*-deuterated **2_{ortho}** as an orange-yellow powder (0.006 g, 87%). ^1H NMR (CDCl_3 , 400 MHz): 1.16 (d, 6H, $^3J_{HH} = 6.8$ Hz, CH(CH₃)₂), 1.39 (d, 6H, $^3J_{HH} = 6.8$ Hz, CH(CH₃)₂), 2.22 (s, 3H, NCCH₃), 3.07 (sept, 2H, $^3J_{HH} = 6.8$ Hz, CH(CH₃)₂), 7.25 (s, 3H, dipp-H), 7.41 (t, 1H, $^3J_{HH} = 7.5$ Hz, Ar-H), 7.49–7.54 (m, 2H, Ar/Py-H), 7.60 (d, 1H, $^3J_{HH} = 8.6$ Hz, Ar-H), 7.84 (d, 1H, $^3J_{HH} = 8.3$ Hz, Ar-H), 8.02 (t, 1H, $^3J_{HH} = 8.3$ Hz, Py-H), 8.20 (d, 1H, $^3J_{HH} = 8.3$ Hz, Ar-H), 8.35 (d, 1H, $^3J_{HH} = 7.4$ Hz, Ar-H).

Thermolysis of 1a in toluene

To a 25 mL round-bottom flask, equipped with a stir bar and open to the air, was added **1a** (0.005 g, 0.009 mmol) and toluene (3 mL). A condenser was attached and the mixture stirred and heated to 100 °C for 24 h. Upon cooling to room temperature, the solvent was removed under reduced pressure. Analysis of the resulting residue by ^1H NMR spectroscopy (CDCl_3) revealed a 55:45 mixture of **2_{ortho}** and **2_{peri}**.

Isomerisation of 2_{peri} to 2_{ortho}

To a 25 mL round-bottom flask, equipped with a stir bar and open to the air, was added **2_{peri}** (0.005 g, 0.009 mmol) and glacial acetic acid (3 mL). A condenser was attached and the mixture stirred and heated to 100 °C for firstly 24 h and then 48 h. After the designated

Conversion of 3_{peri} to 2_{peri}

To a 50 mL round-bottom flask, open to the air and equipped with a magnetic stir bar, was added (L_{Me})PdOAc (**3_{peri}**) (0.051 g, 0.09 mmol), dichloromethane (10 mL) and a saturated aqueous solution of sodium chloride (10 mL). The biphasic mixture was then stirred vigorously overnight to obtain a yellow coloured reaction mixture. The organic phase was then separated and the aqueous layer washed with chloroform (2 x 10 mL). The organic extracts were combined and dried over magnesium sulfate. The solvent was removed under reduced pressure to give **2_{peri}** as a yellow-brown solid (0.053 g, 99%). Single crystals could be grown by layering a dichloromethane solution of the complex with hexane. Mp: > 260 °C. ^1H NMR (CDCl_3 , 400 MHz): δ 1.06 (d, 6H, $^3J_{HH} = 6.9$ Hz, CH(CH₃)₂), 1.35 (d, 6H, $^3J_{HH} = 6.9$ Hz, CH(CH₃)₂), 2.27 (s, 3H, NCCH₃), 3.05 (sept, 2H, $^3J_{HH} = 6.9$ Hz, CH(CH₃)₂), 7.16–7.23 (m, 3H, dipp-H), 7.26 (d, 1H, $^3J_{HH} = 7.6$ Hz, Ar-H) 7.47 (t, 1H, $^3J_{HH} = 7.8$ Hz, Ar-H), 7.58 (d, 1H, $^3J_{HH} = 7.8$ Hz, Ar-H), 7.85 (d, 1H, $^3J_{HH} = 7.6$ Hz, Ar-H), 7.94 (d, 1H, $^3J_{HH} = 8.0$ Hz, Py-H), 8.10 (t, 1H, $^3J_{HH} = 8.0$ Hz, Py-H), 8.15 (d, 1H, $^3J_{HH} = 7.4$ Hz, Ar-H), 8.40 (d, 1H, $^3J_{HH} = 8.0$ Hz, Py-H), 8.61 (d, 1H, $^3J_{HH} = 7.4$ Hz, Ar-H). $^{13}\text{C}\{\text{H}\}$ NMR (CDCl_3 , 100 MHz): δ 18.7 (Py-C(N)-CH₃), 23.8 (Ar-CH-(CH₃)₂), 23.9 (Ar-CH-(CH₃)_{2b}), 28.81 (Ar-CH-(CH₃)₂), 120.2 (CH), 122.8 (CH), 123.3 (CH), 123.4 (C), 123.9 (CH), 125.5 (CH), 126.4 (CH), 127.2 (CH), 128.3 (CH), 129.3 (CH), 133.8 (C), 134.2 (CH), 134.8 (C), 137.3 (C), 139.0 (CH), 141.0 (C), 142.1 (C), 155.6 (C), 156.3 (C), 171.2 (C=N_{imine}). IR (cm^{-1}): 754 $\nu(\text{C}-\text{H bend})$, 795 $\nu(\text{C}-\text{H bend})$, 1591 $\nu(\text{C}-\text{N})_{\text{pyridine}}$, 1627 $\nu(\text{C}=\text{N})_{\text{imine}}$, 2960 $\nu(\text{C}-\text{H stretch})$. ESIMS (+ve, MeOH): *m/z* 547 [M]⁺. HRMS (FAB): calculated for $\text{C}_{29}\text{H}_{29}\text{N}_2\text{PdCl}$ [M]⁺ 547.2023 and $\text{C}_{29}\text{H}_{29}\text{N}_2\text{Pd}$ [M-Cl]⁺ 511.1088, found 547.2017 and

time period, the reaction mixture was cooled to room temperature and the solvent removed under reduced pressure. At 24 h, a 83:17 mixture of **2_{ortho}** and **2_{peri}** was revealed by ¹H NMR spectroscopy (CDCl₃). At 48 h, a 90:10 mixture of **2_{ortho}** and **2_{peri}** was shown by ¹H NMR spectroscopy (CDCl₃).

Crystallographic Studies

Data for **1a**, **1b**, **2_{ortho}** and **2_{peri}** were collected on a Bruker APEX 2000 CCD diffractometer. Details of data collection, refinement and crystal data are listed in Table 4. The data were corrected for Lorentz and polarisation effects and empirical absorption corrections applied. Structure solution by direct methods and structure refinement based on full-matrix least-squares on *F*² employed SHELXTL version 6.10.²² Hydrogen atoms were included in calculated positions (C-H = 0.93 – 1.00 Å) riding on the bonded atom with isotropic displacement parameters set to 1.5 Ueq(C) for methyl H atoms and 1.2 Ueq(C) for all other H atoms. All non-H atoms, were refined with anisotropic displacement parameters. Disordered solvent was omitted using the SQUEEZE option in PLATON for **1b**.²³

Computational methods

Calculations were performed with Gaussian 09, Revision E.01.²⁴ Geometry optimisations and thermal contributions to energies were computed in the gas phase with the gradient-corrected functional BP86²⁵ and employed the SDD basis set for Pd with the Stuttgart/Dresden 28-electron ECP;²⁶ the 6–31G(d,p) basis set was used for all other atoms.²⁷ Stationary points were identified as minima or transition states through analytical frequency calculations; transition states were further characterised through IRC calculations and subsequent geometry optimisations. The energies reported in the main text are Gibbs energies that include both a dispersion correction (Grimme's D3)²⁸ and a solvent correction (AcOH or toluene, PCM approach).²⁹ Structures in the manuscript were produced with CYLview.³⁰ The supplementary information contains computed Cartesian coordinates and energies for all species and details of investigations into other reaction mechanisms.

Conflicts of interest

There are no conflicts to declare.

Acknowledgements

We thank the University of Leicester for financial assistance; we also thank Nottingham Trent University for an Undergraduate Research Studentship for SMG and for the provision of computational resources. Johnson Matthey PLC are thanked for their generous loan of palladium chloride.

Notes and references

- 1 a) B. G. Hashiguchi, S. M. Bischof, M. M. Konnick, R. A. Periana, *Acc. Chem. Res.* 2012, **45**, 885–898; b) A. N. Vedernikov, *Curr. Org. Chem.* 2007, **11**, 1401–1416; c) G. B. Shulpin, *Org. Biomol. Chem.*

- 2010, **8**, 4217–4228; d) X.-S. Xue, P. Ji, B. Zhou, J.-P. Cheng, *Chem. Rev.* 2017, **117**, 8622–8648.
- 2 a) R. H. Crabtree, A. Lei, *Chem. Rev.* 2017, **117**, 8841–8482; b) J. He, M. Wasa, K. S. L. Chan, Q. Shao, J.-Q. Yu, *Chem. Rev.* 2017, **117**, 8754–8786; c) R. Shang, L. Ilies, E. Nakamura, *Chem. Rev.* 2017, **117**, 9086–9138; c) Y. Park, Y. Kim, S. Chang, *Chem. Rev.* 2017, **117**, 9247–9301; d) K. Murakami, S. Yamada, K. Itami, *Chem. Rev.* 2017, **117**, 9302–9332; e) Y. Qin, L. Zhu, S. Luo, *Chem. Rev.* 2017, **117**, 9433–9520.
- 3 C-H Bond Activation in Organic Synthesis (Ed. J. Li), Boca Raton: CRC Press, 2015.
- 4 a) D. Balcells, E. Clot, O. Eisenstein, *Chem. Rev.* 2010, **110**, 749–823. b) O. Eisenstein, J. Milani, R. N. Perutz, *Chem. Rev.* 2017, **117**, 8710–8753; c) K. J. T. Carr, S. Macgregor, C. L. McMullin, *Top. Organomet. Chem.* 2016, **55**, 53–76.
- 5 a) J. Li, S. De Sarkar, L. Ackermann, *Top. Organomet. Chem.* 2015, **55**, 217–257; b) L. Ilies, E. Nakamura, *Top. Organomet. Chem.* 2016, **56**, 1–18; c) D. Dailler, G. Danoun, O. Baudoin, *Top. Organomet. Chem.* 2016, **56**, 133–154; d) F. Shi, R. C. Larock, *Top. Curr. Chem.* 2010, **292**, 123–164; e) O. Daugulis, *Top. Curr. Chem.* 2010, **292**, 57–84.
- 6 a) X. Chen, K. M. Engle, D.-H. Wong, J.-Q. Yu, *Angew. Chem. Int. Ed.* 2009, **48**, 5094–5115; b) J. Dupont, C.S. Consorti, J. Spencer, *Chem. Rev.* 2005, **105**, 2527–2571; c) N. J. Gunsalus, A. Koppaka, S. H. Park, S. M. Bischof, B. G. Hashiguchi, R. A. Periana, *Chem. Rev.* 2017, **117**, 8521–8573; d) R. H. Crabtree, *Chem. Rev.* 2010, **110**, 575–575.
- 7 For selected examples of proximal C-H activation employing a chelating directing group, see: a) T. Lyons, M. Sanford, *Chem. Rev.* 2010, **110**, 1147–1169; b) Y.-J. Liu, H. Xu, W.-J. Kong, M. Shang, H.-X. Dai, J.-Q. Yu, *Nature* 2014, **515**, 389–393.
- 8 For selected examples of remote C-H activation employing a chelating directing group, see: a) Z. Zhang, K. Tanaka, J.-Q. Yu, *Nature* 2017, **543**, 538–542; b) R.-Y. Tang, G. Li, J.-Q. Yu, *Nature* 2014, **507**, 215–220; c) G.-J. Cheng, Y.-F. Yang, P. Liu, P. Chen, T.-Y. Sun, G. Li, X. Zhang, K. N. Houk, J.-Q. Yu, Y.-D. Wu, *J. Am. Chem. Soc.* 2014, **136**, 894–897; d) D. Leow, G. Li, T.-S. Mei, J.-Q. Yu, *Nature* 2012, **486**, 518–522.
- 9 a) N. Kuhl, M. N. Hopkinson, J. Wencel-Delord, F. Glorius, *Angew. Chem. Int. Ed. Engl.* 2012, **51**, 10236–10254; b) B. Liégault, I. Petrov, S. I. Gorelsky, K. Fagnou, *J. Org. Chem.* 2010, **75**, 1047–1060; c) D. Lapointe, T. Markiewicz, C. J. Whipp, A. Toderian, K. Fagnou, *J. Org. Chem.* 2011, **76**, 749–759.
- 10 For example, see: a) S. Yanagisawa, K. Ueda, H. Sekizawa, K. Itami, *J. Am. Chem. Soc.* 2009, **131**, 14622–14623; b) J. D. Dooley, S. Reddy Chidipudi, H. W. Lam, *J. Am. Chem. Soc.* 2013, **135**, 10829–10836.
- 11 For example, see: a) D. L. Davies, C. E. Ellul, S. A. Macgregor, C. L. McMullin, K. Singh, *J. Am. Chem. Soc.* 2015, **137**, 9659–9669; b) A. W. Garner, C. F. Harris, D. A. K. Vezzu, R. D. Pike, S. Huo, *Chem. Commun.* 2011, **47**, 1902–1904; c) D. Vázquez-García, A. Fernández, M. López-Torres, A. Rodríguez, N. Gómez-Blanco, C. Viader, J. M. Vila, J. J. Fernández, *Organometallics* 2010, **29**, 3303–3307.
- 12 W. B. Cross, E.G. Hope, Y.-H. Lin, S. A. MacGregor, K. Singh, G. A. Solan, N. Yahya, *Chem. Commun.* 2013, **49**, 1918–1920.
- 13 a) Y. Boutadla, D. L. Davies, S. A. Macgregor, A. I. Poblador-Bahamonde, *Dalton Trans.* 2009, 5820–5893; b) D. L. Davies, S. M. A. Donald, S. A. Macgregor, *J. Am. Chem. Soc.* 2005, **127**, 13754–13755; c) D. L. Davies, S. A. Macgregor, C. L. McMullin, *Chem. Rev.* 2017, **117**, 8649–8709.

ARTICLE

Journal Name

- 14 a) L. Kind, A. J. Klaus, P. Rys, V. Gramlich, *Helv. Chim. Acta* 1988, **81**, 307-316; b) P.A. Ruppen, PhD thesis No. 8080, ETH-Zurich, 1986.
- 15 J. Albert, R. Bosque, J. M. Cadena, S. Delgado, J. Granell, *J. Organomet. Chem.* 2001, **634**, 83-89.
- 16 a) D. Kalyani, A. R. Dick, W. Q. Anani, M. S. Sanford, *Tetrahedron* 2006, **62**, 11483-11498; b) M. Kondrashov, S. Raman, O. F. Wendt, *Chem. Commun.* 2015, **51**, 911-913.
- 17 a) T. V. Laine, U. Piironen, K. Lappalainen, M. Klinga, E. Aitola, M. Leskela, *J. Organomet. Chem.*, 2000, **606**, 112-124; b) W. M. Motswainyana, M. O. Onani, A. M. Madiehe, M. Saibu, J. Jacobs, L. van Meervelt, *Inorg. Chim. Acta* 2013, **400**, 197-202; c) J. Kuwabara, D. Takeuchi, K. Osakada, *Polyhedron* 2009, **28**, 2459-2465; d) T. Irrgang, S. Keller, H. Maisel, W. Kretschmer, R. Kempe, *Eur. J. Inorg. Chem.* 2007, 4221-4228; e) T. V. Laine, M. Klinga, M. Leskela, *Eur. J. Inorg. Chem.* 1999, 959-964.
- 18 a) C. Bianchini, G. Lenoble, W. Oberhauser, S. Parisel, F. Zanobini, *Eur. J. Inorg. Chem.* 2005, 4794-4800; b) Q. Mahmood, E. Yue, W. Zhang, G. A. Solan, T. Liang, W.-H. Sun, *Org. Chem. Fronts.* 2016, **3**, 1668-1679; c) R. Simayi, E. G. Hope, K. Singh, W. B. Cross, G. A. Solan, *J. Organomet. Chem.* 2017, **851**, 254-264.
- 19 a) Z. Ke, T. R. Cundari, *Organometallics* 2010, **29**, 821-834; b) A. K. Sharma, D. Roy, R. B. Sunoj, *Dalton Trans.* 2014, **43**, 10183-10201.
- 20 a) L. Goerigk, S. Grimme, *Phys. Chem. Chem. Phys.* 2011, **13**, 6670-6688; (b) G. N. Simm, M. Reiher, *J. Chem. Theory Comput.* 2016, **12**, 2762-2773.
- 21 F. Ozawa, in: *Synthesis of Organometallic compounds: A Practical Guide* (Ed.: S. Komiya), John Wiley & Sons, 1997, pp 249-303.
- 22 G. M. Sheldrick, SHELXTL Version 6.10. Bruker AXS, Inc. Madison, Wisconsin, USA, 2000.
- 23 A. L. Spek, *Acta Cryst. Sect C* 2015, **71**, 9-18.
- 24 Gaussian 09 (Revision E.01), M. J. Frisch, G. W. Trucks, H. B. Schlegel, G. E. Scuseria, M. A. Robb, J. R. Cheeseman, G. Scalmani, V. Barone, B. Mennucci, G. A. Petersson, H. Nakatsuji, M. Caricato, X. Li, H. P. Hratchian, A. F. Izmaylov, J. Bloino, G. Zheng, J. L. Sonnenberg, M. Hada, M. Ehara, K. Toyota, R. Fukuda, J. Hasegawa, M. Ishida, T. Nakajima, Y. Honda, O. Kitao, H. Nakai, T. Vreven, J. A. Montgomery, Jr., J. E. Peralta, F. Ogliaro, M. Bearpark, J. J. Heyd, E. Brothers, K. N. Kudin, V. N. Staroverov, T. Keith, R. Kobayashi, J. Normand, K. Raghavachari, A. Rendell, J. C. Burant, S. S. Iyengar, J. Tomasi, M. Cossi, N. Rega, J. M. Millam, M. Klene, J. E. Knox, J. B. Cross, V. Bakken, C. Adamo, J. Jaramillo, R. Gomperts, R. E. Stratmann, O. Yazyev, A. J. Austin, R. Cammi, C. Pomelli, J. W. Ochterski, R. L. Martin, K. Morokuma, V. G. Zakrzewski, G. A. Voth, P. Salvador, J. J. Dannenberg, S. Dapprich, A. D. Daniels, O. Farkas, J. B. Foresman, J. V. Ortiz, J. Cioslowski, and D. J. Fox, Gaussian, Inc., Wallingford CT, 2013.
- 25 a) A.D. Becke, *Phys. Rev. A* 1988, **38**, 3098-3100; b) J. P. Perdew, *Phys. Rev. B* 1986, **33**, 8822-8824.
- 26 D. Andrae, U. Haeussermann, M. Dolg, H. Stoll, H. Preuss, *Theor. Chem. Acc.* **1990**, *77*, 123-124.
- 27 a) W. J. Hehre, R. Ditchfield, J. A. Pople, *J. Chem. Phys.* 1972, **56**, 2257-2261; b) P. C. Hariharan, J. A. Pople, *Theor. Chem. Acta* 1973, **28**, 213-222.
- 28 S. Grimme, J. Antony, S. Ehrlich, H. Krieg, *J. Chem. Phys.* 2010, **132**, 154104-154194.
- 29 J. Tomasi, B. Mennucci, R. Cammi, *Chem. Rev.* 2005, **105**, 2999-3093.
- 30 CYLview, 1.0b; C. Y. Legault, Université de Sherbrooke, 2009 (<http://www.cylview.org>)

Supporting information

Ligand and solvent control of selectivity in the C-H activation of a pyridylimine-substituted 1-naphthalene; a combined synthetic and computational study

Rena Simayi,^a Simone M. Gillbard,^b Warren B. Cross,^{b,*} Eric G. Hope,^a
Kuldip Singh and Gregory A. Solan^{a,*}

^a Department of Chemistry, University of Leicester, University Road, Leicester LE1 7RH, UK

^b School of Science and Technology, Nottingham Trent University, Clifton Lane, Nottingham NG11 8NS, UK

* Corresponding authors: gas8@leicester.ac.uk (G.A. Solan), warren.cross@ntu.ac.uk (W.B. Cross)

CONTENTS**Part A**

1. **Figure S1** ORTEP representation of **1a**
2. **Table S1** Selected bond distances (\AA) and angles ($^\circ$) for **1a**
3. **Figure S2** ^1H NMR spectrum of **1a** in CDCl_3 at room temperature
4. **Figure S3** ^1H NMR spectrum of **1b** in CD_2Cl_2 at room temperature
5. **Figure S4a** ^1H NMR spectrum of **2_{ortho}** in CDCl_3 at room temperature
6. **Figure S4b** COSY spectrum of **2_{ortho}** in CDCl_3 at room temperature
7. **Figure S5** ^1H NMR spectrum of **2_{peri}** in CDCl_3 at room temperature
8. **Figure S5b** COSY spectrum of **2_{peri}** in CDCl_3 at room temperature
9. **Figure S6** ^1H NMR spectrum of **3_{peri}·AgCl** in CDCl_3 at room temperature; recorded in CDCl_3 at room temperature
10. **Figure S7** Side-by-side ^1H NMR spectra for **2_{ortho}** and *peri*-deuterated **2_{ortho}**
11. **Figure S8** ^1H NMR spectra in the 2.8 – 4.0 ppm region of (a) **2_{ortho}**, (b) **2_{peri}**, (c) **1a**, (d) after heating **1a** in toluene for 12 h at 60 °C, (e) after heating **1a** in toluene for 24 h at 100 °C; all recorded in CDCl_3 at room temperature
12. **Figure S9** Aryl region of ^1H NMR spectra of (a) **2_{ortho}**, (b) after heating **2_{ortho}** for 24 h at 100 °C in acetic acid and (c) after heating **2_{ortho}** at 100 °C for 48 h in acetic acid; all recorded in CDCl_3 at room temperature
13. **Figure S10** ^1H NMR spectra in the 2.8 – 4.0 ppm region of (a) **2_{peri}**, (b) **2_{ortho}**, (c) **1a**, (d) heating **1a** in acetic acid for 60 h at 100 °C, (e) **1a**; all recorded in CDCl_3 at room temperature

Part B

1. Computational methods
2. **Figure S11.** Computed reaction profile for the C-H activation of **1a** via an **inner-sphere concerted-metallation-deprotonation mechanism**. Energies were calculated at the BP86+D3/SDD/6-31G(d,p) level and include a PCM solvent correction in acetic acid or toluene (parentheses).
3. **Table S1.** Computed relative energies for the C-H activation of **1a** via an **inner-sphere concerted-metallation-deprotonation mechanism**.
4. **Figure S12.** Computed reaction profile for the C-H activation of **1a** via an **outer-sphere concerted-metallation-deprotonation mechanism**.
5. **Table S2.** Computed relative energies for the C-H activation of **1a** via an **outer-sphere concerted-metallation-deprotonation mechanism**.
6. **Figure S13.** Computed reaction profile for the C-H activation of **1a** via an **oxidative addition mechanism**.
7. **Table S3.** Computed relative energies for the C-H activation of **1a** via an **oxidative addition mechanism**.
8. **Table S4.** DFT method testing
9. Computed structures and energies (hartrees) for all species computed

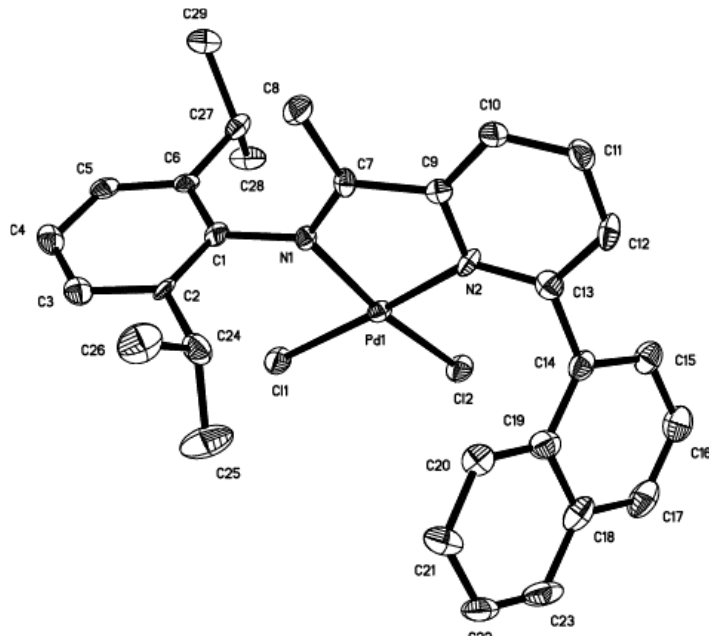
PART A

Figure S1 ORTEP representation of **1a** with thermal ellipsoids set at 50% probability level; all hydrogen atoms are omitted for clarity.

Table S1 Selected bond distances (\AA) and angles ($^\circ$) for **1a**

<i>Bond lengths</i>	
Pd(1)-N(2)	2.059(6)
Pd(1)-N(1)	2.010(6)
Pd(1)-Cl(2)	2.298(2)
Pd(1)-Cl(1)	2.270(2)
C(7)-N(1)	1.295(9)
C(13)-C(14)	1.518(11)

<i>Bond angles</i>	
N(2)-Pd(1)-Cl(2)	99.34(18)
N(2)-Pd(1)-Cl(1)	172.77(19)
N(2)-Pd(1)-N(1)	80.4(3)
N(1)-Pd(1)-Cl(2)	169.26(18)
N(1)-Pd(1)-Cl(1)	93.56(19)
Cl(1)-Pd(1)-Cl(2)	87.34(8)
C(7)-N(1)-C(1)	120.7(7)

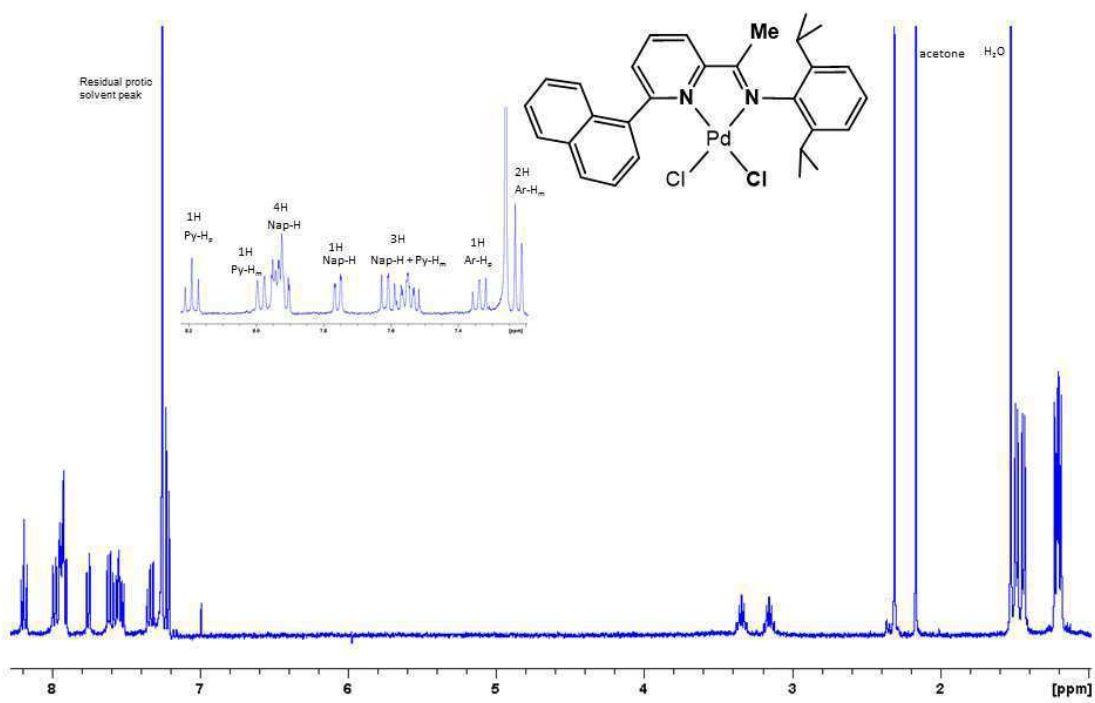


Figure S2 ^1H NMR spectrum of **1a** in CDCl_3 at room temperature

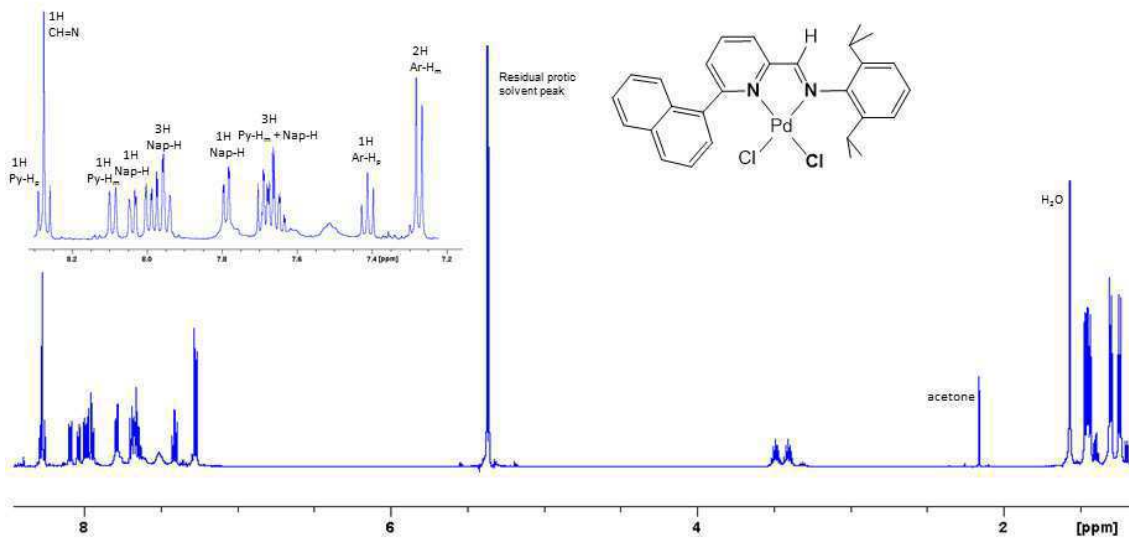


Figure S3 ^1H NMR spectrum of **1b** in CD_2Cl_2 at room temperature

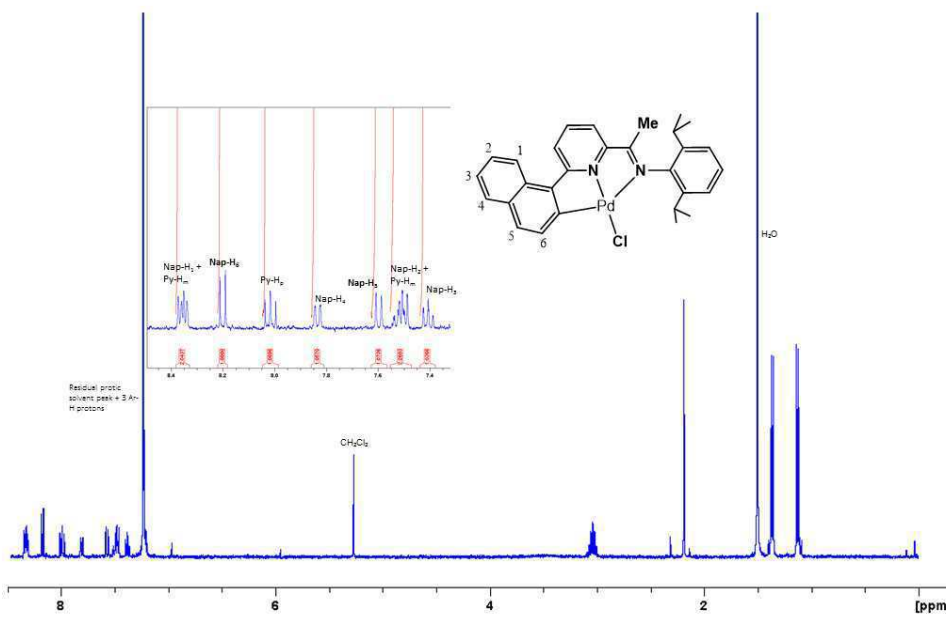


Figure S4a ^1H NMR spectrum of $\mathbf{2}_{\text{ortho}}$ in CDCl_3 at room temperature

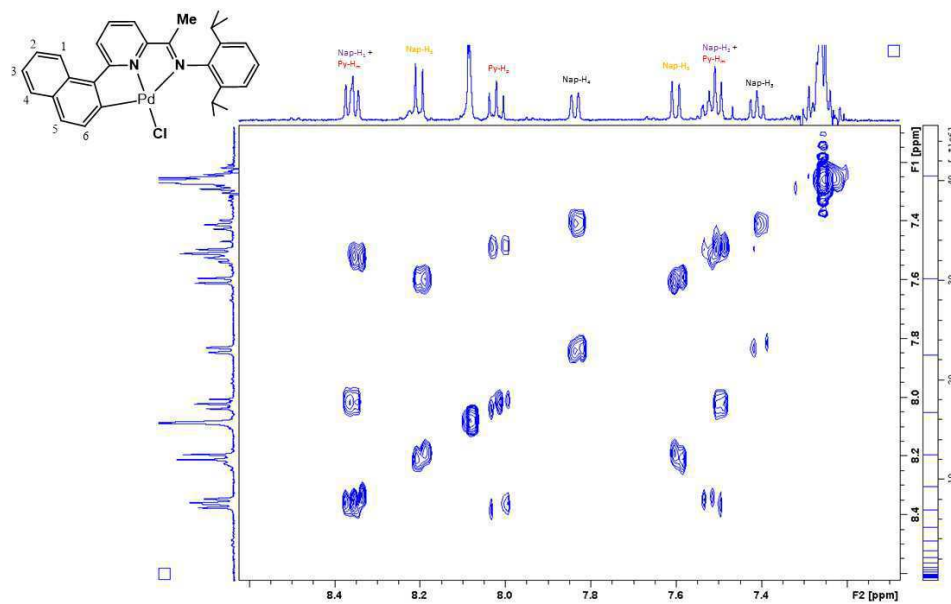


Figure S4b COSY spectrum of the aromatic region in $\mathbf{2}_{\text{ortho}}$ in CDCl_3 at room temperature

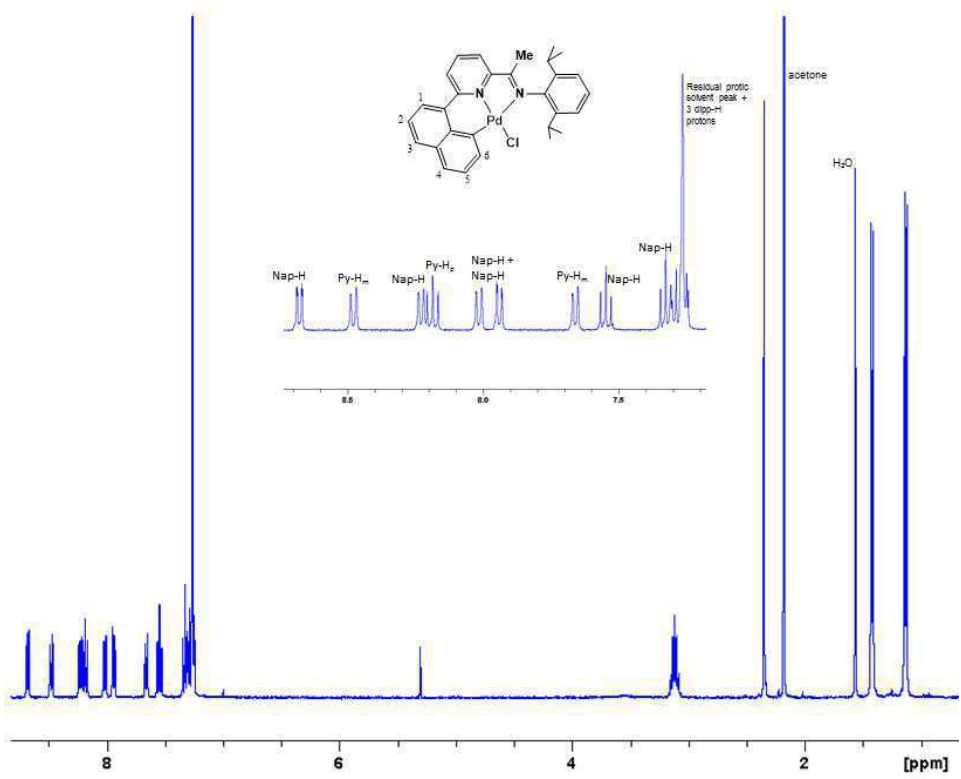


Figure S5a ^1H NMR spectrum of $\mathbf{2}_{\text{peri}}$ in CDCl_3 at room temperature

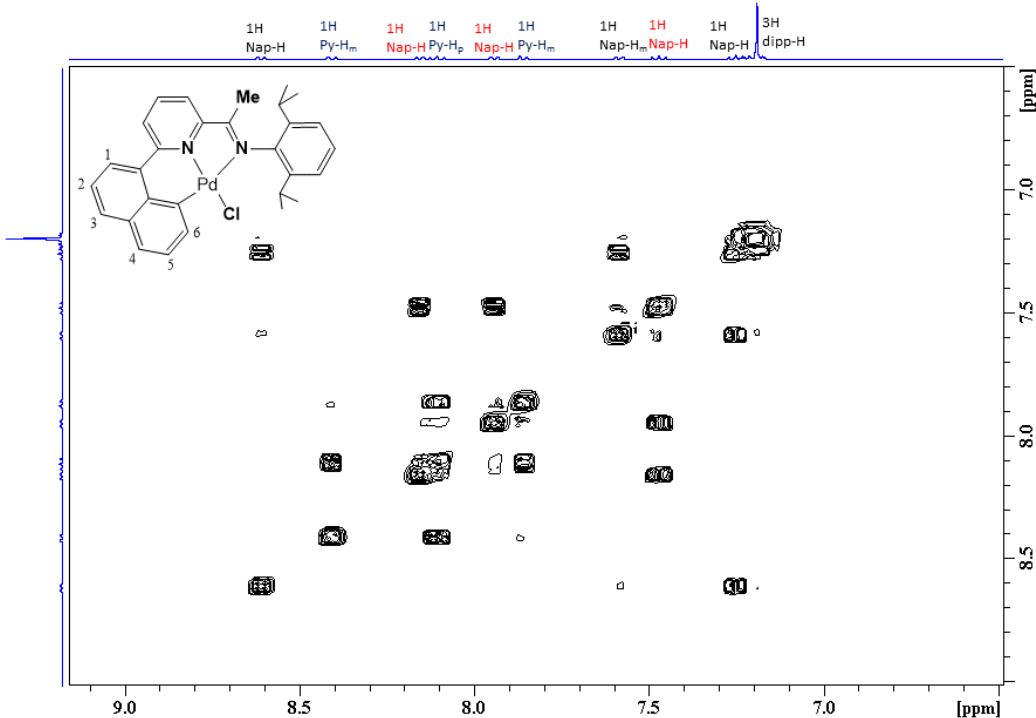


Figure S5b COSY spectrum of the aromatic region in $\mathbf{2}_{\text{peri}}$ in CDCl_3 at room temperature

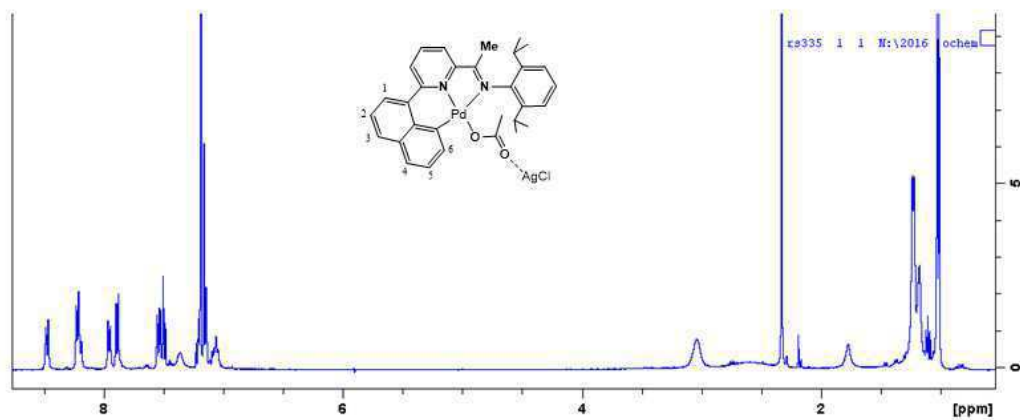


Figure S6 ¹H NMR spectrum of **3_{peri}**·AgCl in CDCl_3 at room temperature

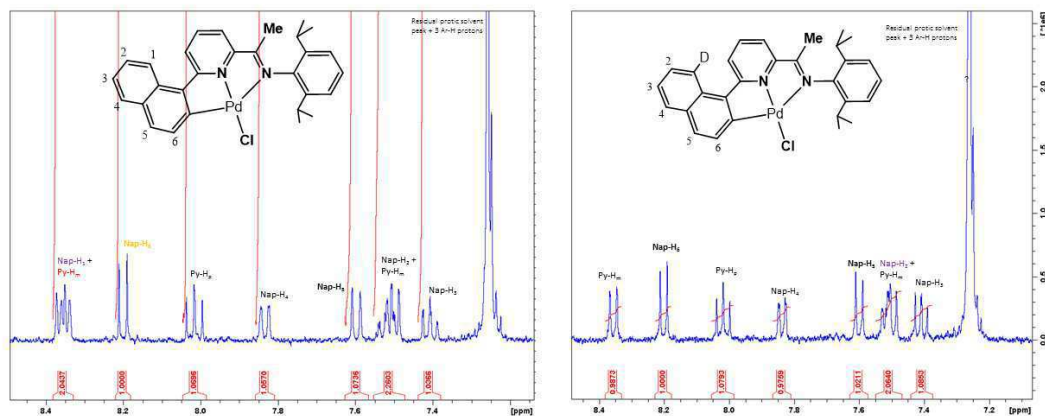


Figure S7 Side-by-side ¹H NMR spectra for **2_{ortho}** and *peri*-deuterated **2_{ortho}**

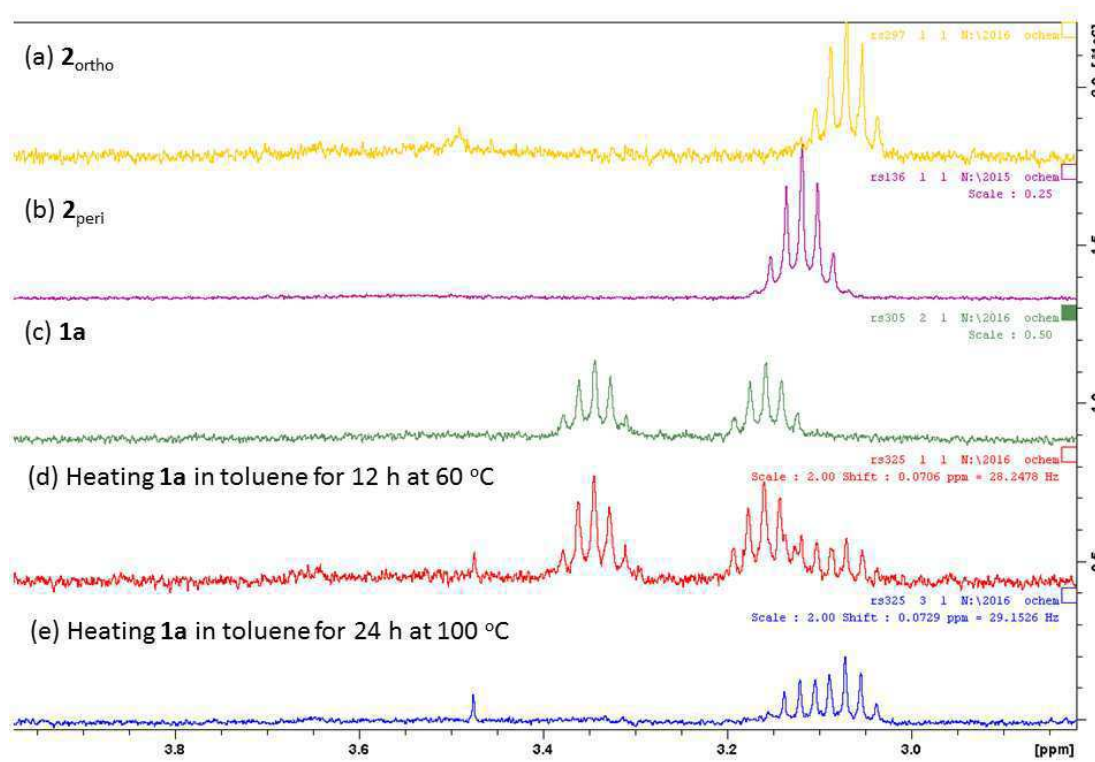


Figure S8 ¹H NMR spectra in the 2.8 – 4.0 ppm region of (a) 2_{ortho}, (b) 2_{peri}, (c) 1a, (d) heating 1a in toluene for 12 h at 60 °C, (e) heating 1a in toluene for 24 h at 100 °C; all recorded in CDCl₃

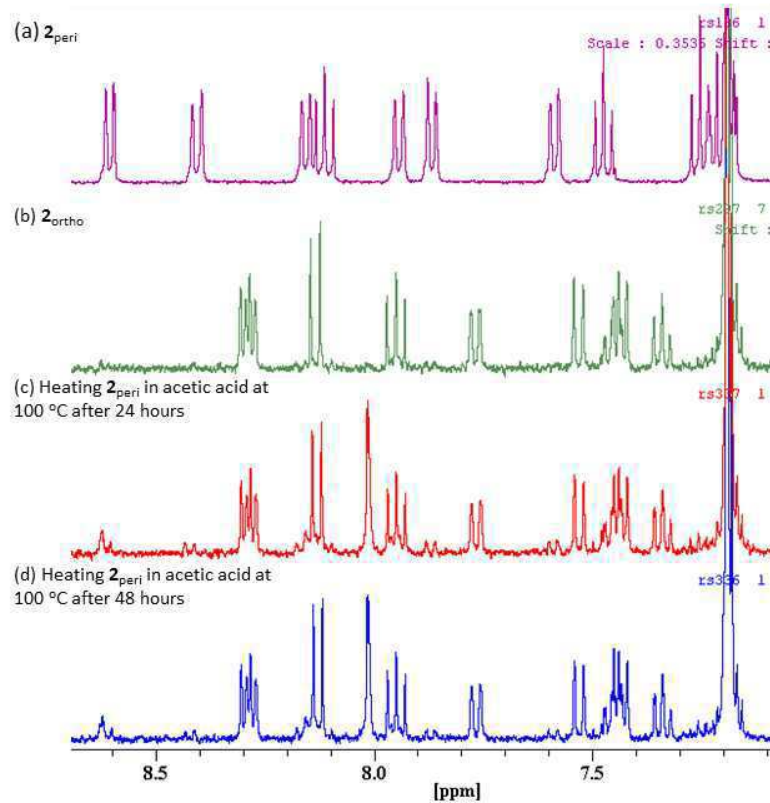


Figure S9 Aryl region of ¹H NMR spectra of (a) 2_{peri}, (b) 2_{ortho}, (c) after heating 2_{peri} for 24 h at 100 °C in acetic acid and (d) after heating 2_{ortho} at 100 °C for 48 h in acetic acid; all recorded in CDCl₃

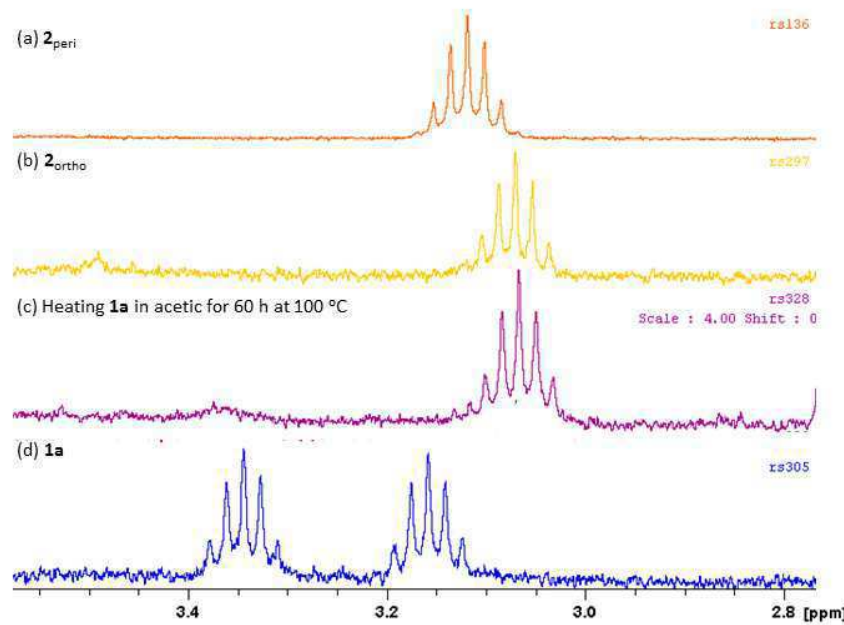


Figure S10 ^1H NMR spectra in the 2.8 – 4.0 ppm region of (a) $\mathbf{2}_{\text{peri}}$, (b) $\mathbf{2}_{\text{ortho}}$, (c) $\mathbf{1}\mathbf{a}$, (d) heating $\mathbf{1}\mathbf{a}$ in acetic acid for 60 h at 100 °C, (e) $\mathbf{1}\mathbf{a}$; all recorded in CDCl_3 at room temperature

PART B

Computational Methods

Calculations were performed with Gaussian 09, Revision E.01.^{S1} Geometry optimizations and thermal contributions to energies were computed in the gas phase with the gradient-corrected functional BP86^{S2} and employed the SDD basis set for Pd with the Stuttgart/Dresden 28-electron ECP,^{S3} the 6–31G(d,p) basis set was used for all other atoms.^{S4} Stationary points were identified as minima or transition states through analytical frequency calculations; transition states were further characterised through IRC calculations and subsequent geometry optimisations. The energies reported in the main text are Gibbs energies that include both a dispersion correction (Grimme's D3)^{S5} and a solvent correction (AcOH or toluene, PCM approach).^{S6}

Whereas C-H activation mediated by palladium carboxylate complexes has been thoroughly investigated by computational methods, C-H activation by palladium chloride complexes has been less well studied.^{S7} Therefore all plausible mechanisms for the C-H activation of complex $\mathbf{1}\mathbf{a}$ were investigated, including:

Fig. S11 and Table S1: concerted-metallation-deprotonation, involving an inner-sphere chloride ligand

Fig. S12 and Table S2: concerted-metallation-deprotonation, involving an outer-sphere chloride anion

Fig. S13 and Table S3: oxidative addition.

The concerted-metallation-deprotonation mechanism, involving an inner-sphere chloride ligand proved to be the lowest energy pathway; hence, this mechanism is the one presented in the main text.

A study testing the computational method was undertaken, see **Table S4**.

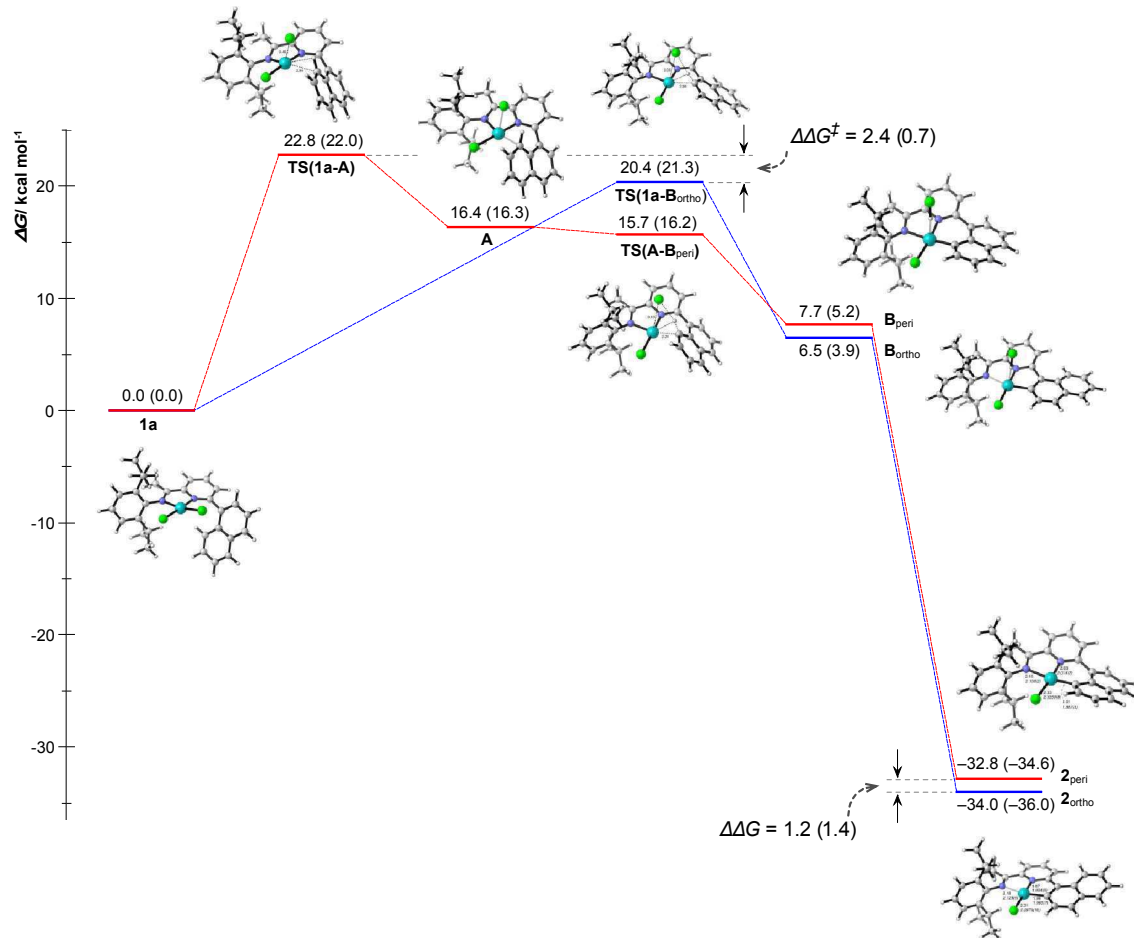


Figure S11. Computed reaction profile for the C-H activation of **1a** via an **inner-sphere concerted-metallation-deprotonation mechanism**. Energies were calculated at the BP86+D3/SDD/6-31G(d,p) level and include a PCM solvent correction in acetic acid or toluene (parentheses).

Table S1. Computed relative energies for the C-H activation of **1a** via an **inner-sphere concerted-metallation-deprotonation mechanism**. Energies were calculated at the BP86+D3/SDD/6-31G(d,p) level and include a PCM solvent correction. Data in bold are those used in the main text.

	Solvent = AcOH					Solvent = PhMe				
	SCF energy	SCF + ZP energy	SCF + thermal energy	SCF + thermal enthalpy	SCF + thermal free energy	SCF energy	SCF + ZP energy	SCF + thermal energy	SCF + thermal enthalpy	SCF + thermal free energy
1a	0.0	0.0	0.0	0.0	0.0	0.0	0.0	0.0	0.0	0.0
TS(1a-A)	22.3	21.8	21.4	21.4	22.8	21.5	21.0	20.6	20.6	22.0
A	16.2	15.6	15.7	15.7	16.4	16.1	15.5	15.6	15.6	16.3
TS(A-B_{peri})	15.2	14.1	13.7	13.7	15.7	15.6	14.6	14.2	14.2	16.2
TS(1a-B_{ortho})	21.7	20.1	19.9	19.9	20.4	22.6	21.0	20.8	20.8	21.3
B_{ortho}	10.4	7.5	7.8	7.8	6.5	7.8	5.0	5.3	5.3	3.9
B_{peri}	10.1	7.5	7.6	7.6	7.7	7.6	5.0	5.1	5.1	5.2
2_{ortho} + HCl	21.3	17.5	39.1	40.3	-34.0	19.3	15.5	37.1	38.3	-36.0
2_{peri} + HCl	21.9	18.2	39.7	40.9	-32.8	20.0	16.4	37.8	39.0	-34.6

* in the gas phase, **A** is lower in energy than **TS(A-B_{peri})**, including with the dispersion correction; when the solvent correction is applied, **A** is higher in energy than **TS(A-B_{peri})**.

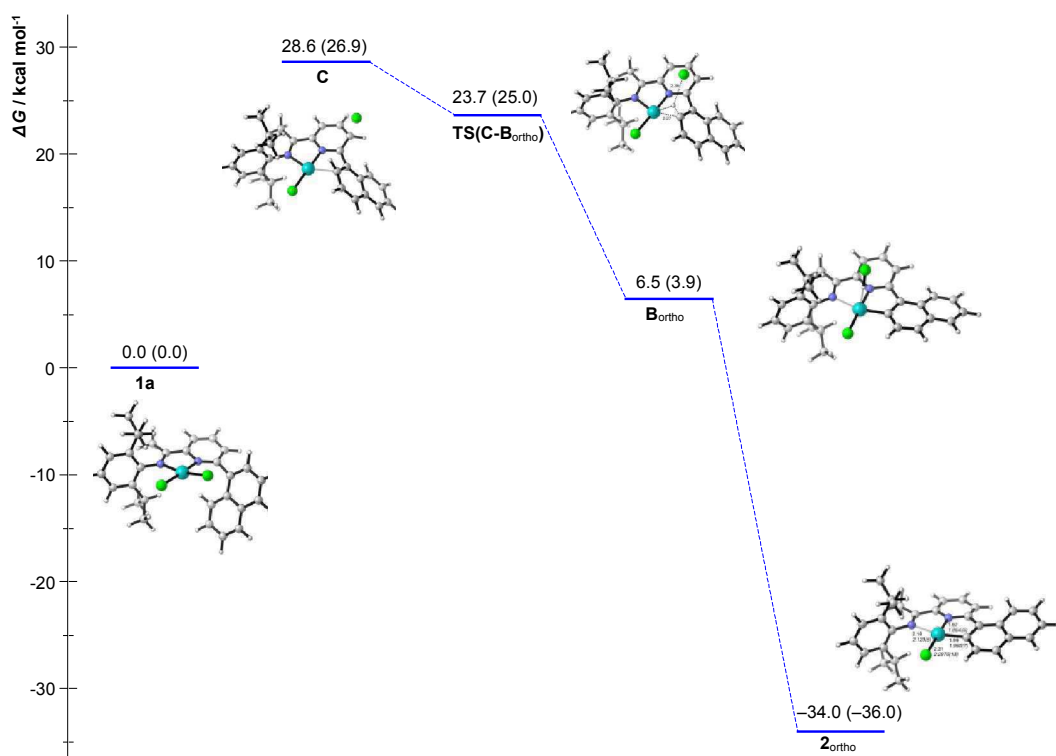


Figure S12. Computed reaction profile for the C-H activation of **1a** via an **outer-sphere concerted-metallation-deprotonation mechanism**. A pathway for the *ortho*-C-H activation only could be located. Energies were calculated at the BP86+D3/SDD/6-31G(d,p) level and include a PCM solvent correction for acetic acid or toluene (parentheses).

Table S2. Computed relative energies for the C-H activation of **1a** via an **outer-sphere concerted-metallation-deprotonation mechanism**. Energies were calculated at the BP86+D3/SDD/6-31G(d,p) level and include a PCM solvent correction.

	Solvent = AcOH					Solvent = PhMe				
	SCF energy	SCF + ZP energy	SCF + thermal energy	SCF + thermal enthalpy	SCF + thermal free energy	SCF energy	SCF + ZP energy	SCF + thermal energy	SCF + thermal enthalpy	SCF + thermal free energy
		0.0	0.0	0.0	0.0		0.0	0.0	0.0	0.0
1a	0.0	0.0	0.0	0.0	0.0	0.0	0.0	0.0	0.0	0.0
C	30.1	29.3	29.6	29.6	28.6	28.3	27.6	27.8	27.8	26.9
TS(C-B_{ortho})	24.7	23.5	23.2	23.2	23.7	26.0	24.7	24.5	24.5	25.0
B_{ortho}	10.4	7.5	7.8	7.8	6.5	7.8	5.0	5.3	5.3	3.9
2_{ortho} + HCl	21.3	17.5	39.1	40.3	-34.0	19.3	15.5	37.1	38.3	-36.0

* in the gas phase, **C** is lower in energy than **TS(C-B_{ortho})**, including with the dispersion correction; when the solvent correction is applied, **C** is higher in energy than **TS(C-B_{ortho})**.

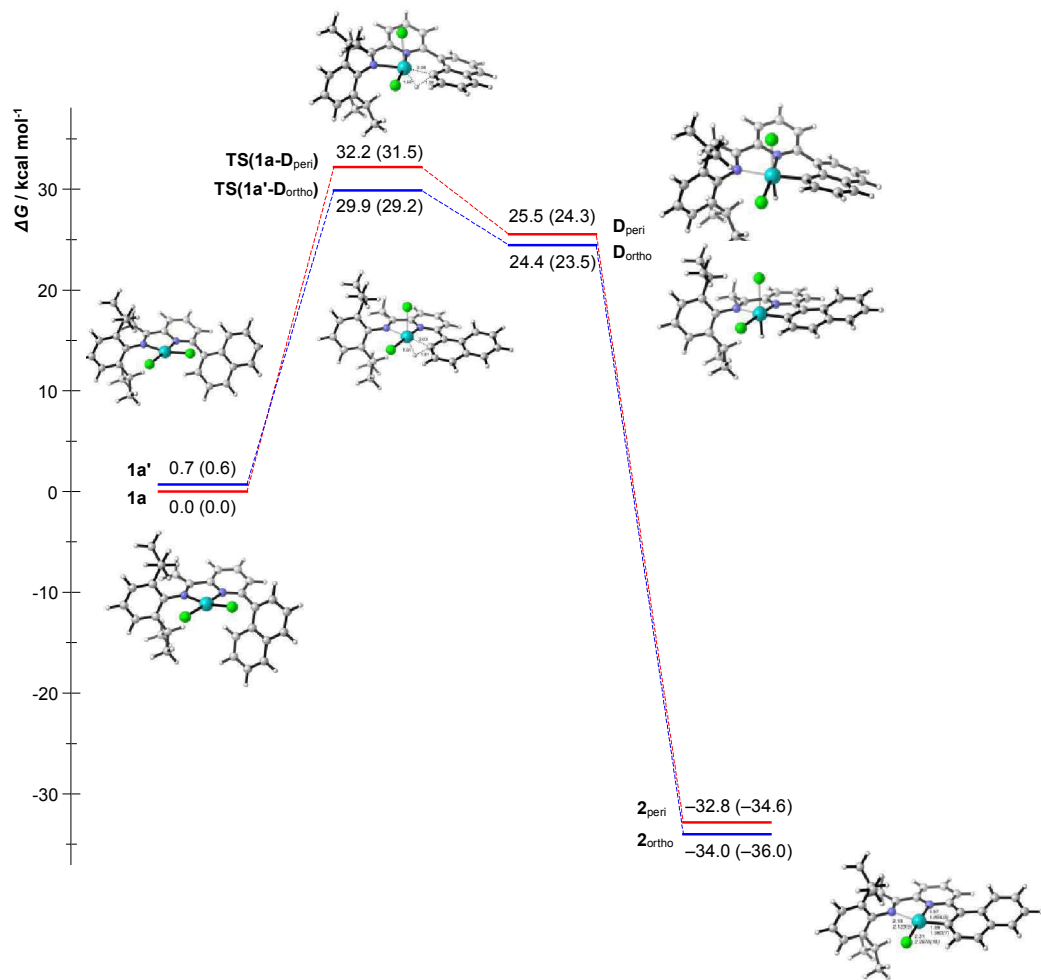


Figure S13. Computed reaction profile for the C-H activation of **1a** via an **oxidative addition mechanism**. Energies were calculated at the BP86+D3/SDD/6-31G(d,p) level and include a PCM solvent correction for acetic acid or toluene (parentheses).

Table S3. Computed relative energies for the C-H activation of **1a** via an **oxidative addition mechanism**. Energies were calculated at the BP86+D3/SDD/6-31G(d,p) level and include a PCM solvent correction.

	Solvent = AcOH					Solvent = PhMe				
	SCF energy	SCF + ZP energy	SCF + thermal energy	SCF + thermal enthalpy	SCF + thermal free energy	SCF energy	SCF + ZP energy	SCF + thermal energy	SCF + thermal enthalpy	SCF + thermal free energy
1a	0.0	0.0	0.0	0.0	0.0	0.0	0.0	0.0	0.0	0.0
1a'	0.7	0.7	0.7	0.7	0.7	0.6	0.6	0.6	0.6	0.6
TS(1a'-D_{ortho})	32.1	29.0	28.8	28.8	29.9	31.5	28.3	28.1	28.1	29.2
TS(1a-D_{peri})	33.8	30.7	30.4	30.4	32.2	33.1	30.1	29.7	29.7	31.5
D_{ortho}	25.4	23.5	23.4	23.4	24.4	24.4	22.6	22.5	22.5	23.5
D_{peri}	25.5	23.7	23.5	23.5	25.5	24.3	22.6	22.3	22.3	24.3
2_{ortho} + HCl	21.3	17.5	39.1	40.3	-34.0	19.3	15.5	37.1	38.3	-36.0
2_{peri} + HCl	21.9	18.2	39.7	40.9	-32.8	20.0	16.4	37.8	39.0	-34.6

Table S4. Method testing: relative computed energies for the C-H activation of **1a**; energies are Gibbs free energies in kcal/mol.

Single-point calculations at the *M06/def2-TZVP//BP86/SDD/6-31G(d,p) + D3 + solvent* level broadly show the same trends as the *BP86/SDD/6-31G(d,p) + D3 + solvent* calculations reported in the main text; however, the former calculations gave higher energy transition state energies that are inconsistent with the experimental conditions under which the reactions were conducted.

Inner-sphere CMD mechanism									
	1a	TS(1a-A)	A	TS(A-B_{peri})	TS(1a-B_{ortho})	B_{ortho}	B_{peri}	Z_{ortho} + HCl	Z_{peri} + HCl
BP86/SDD/6-31G(d,p)	0	21.3	19.0	19.9	22.4	-0.8	2.7	-47.4	-44.0
BP86/SDD/6-31G(d,p) + D3	0	21.4	16.5	17.5	23.0	1.2	2.5	-38.1	-36.6
M06/def2-TZVP//BP86/SDD/6-31G(d,p)	0	26.2	22.3	21.8	28.6	7.9	9.6	-36.3	-34.9
M06/def2-TZVP//BP86/SDD/6-31G(d,p) + D3	0	26.4	22.3	21.8	29.0	8.2	9.5	-34.5	-33.3
BP86/SDD/6-31G(d,p) + D3 + AcOH	0	22.8	16.4	15.7	20.4	6.5	7.7	-34.0	-32.8
M06/def2-TZVP//BP86/SDD/6-31G(d,p) + D3 + AcOH	0	27.8	21.1	19.3	25.2	14.2	15.5	-29.5	-29.2
BP86/SDD/6-31G(d,p) + D3 + PhMe	0	22.0	16.3	16.2	21.3	3.9	5.2	-36.0	-34.6
M06/def2-TZVP//BP86/SDD/6-31G(d,p) + D3 + PhMe	0	27.0	21.4	20.0	26.5	11.3	12.7	-24.4	-23.3

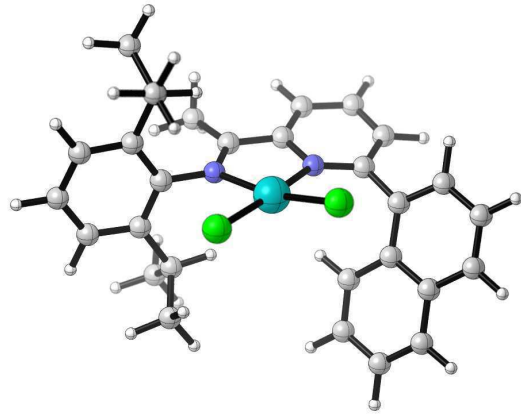
Outer-sphere CMD mechanism					
	1a	C	TS(C-B_{ortho})	B_{ortho}	Z_{ortho} + HCl
BP86/SDD/6-31G(d,p)	0	22.4	26.4	-0.8	-47.4
BP86/SDD/6-31G(d,p) + D3	0	25.8	27.6	1.2	-38.1
M06/def2-TZVP//BP86/SDD/6-31G(d,p)	0	33.1	33.0	7.9	-36.3
M06/def2-TZVP//BP86/SDD/6-31G(d,p) + D3	0	33.8	33.5	8.2	-34.5
BP86/SDD/6-31G(d,p) + D3 + AcOH	0	28.6	23.7	6.5	-34.0
M06/def2-TZVP//BP86/SDD/6-31G(d,p) + D3 + AcOH	0	37.1	28.4	14.2	-29.5
BP86/SDD/6-31G(d,p) + D3 + PhMe	0	26.9	25.0	3.9	-36.0
M06/def2-TZVP//BP86/SDD/6-31G(d,p) + D3 + PhMe	0	35.2	30.1	11.3	-24.4

Table S4 continued. Method testing: relative computed energies for the C-H activation of **1a**; energies are Gibbs free energies in kcal/mol.**Oxidative addition mechanism**

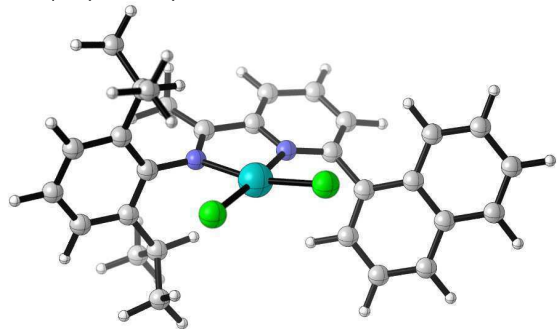
	1a	1a'	TS(1a'-D:ortho)	TS(1a-D:peri)	D:ortho	D:peri	2:ortho + HCl	2:peri + HCl
BP86/SDD/6-31G(d,p)	0	-1.3	27.7	32.5	22.1	25.3	-47.4	-44.0
BP86/SDD/6-31G(d,p) + D3	0	0.7	28.6	30.9	22.7	23.2	-38.1	-36.6
M06/def2-TZVP//BP86/SDD/6-31G(d,p)	0	0.2	41.4	44.7	39.7	40.7	-36.3	-34.9
M06/def2-TZVP//BP86/SDD/6-31G(d,p) + D3	0	0.8	41.9	44.8	40.1	40.7	-34.5	-33.3
BP86/SDD/6-31G(d,p) + D3 + AcOH	0	0.7	29.9	32.2	24.4	25.5	-34.0	-32.8
M06/def2-TZVP//BP86/SDD/6-31G(d,p) + D3 + AcOH	0	0.9	43.6	46.3	42.6	43.8	-29.5	-29.2
BP86/SDD/6-31G(d,p) + D3 + PhMe	0	0.6	29.2	31.5	23.5	24.3	-36.0	-34.6
M06/def2-TZVP//BP86/SDD/6-31G(d,p) + D3 + PhMe	0	0.8	42.7	45.5	41.3	42.3	-24.4	-23.3

Computed Structures and energies (hartrees) for all species computed

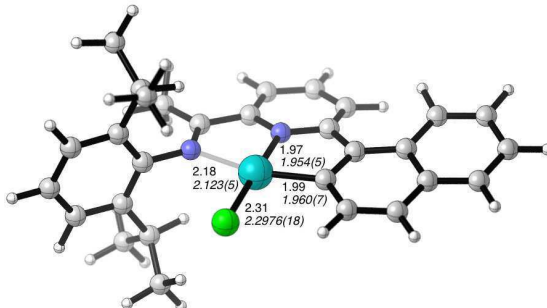
Cartesian coordinates are placed in a separate text file for convenient visualization

1a, (HL:Me) PdCl₂,

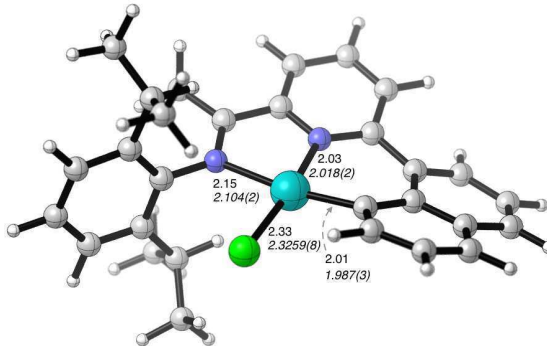
SCF Energy (gas phase)=
-2281.22921882
Zero-point correction= 0.505339
(Hartree/Particle)
Thermal correction to Energy =
0.539722
Thermal correction to Enthalpy =
0.540666
Thermal correction to Gibbs Free
Energy = 0.438184
SCF Energy (AcOH + D3) =
-2281.36140360
SCF Energy (PhMe + D3) =
-2281.34989147

1a', (HL:Me) PdCl₂

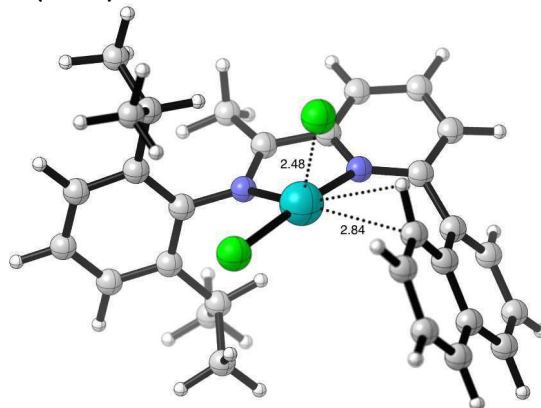
SCF Energy (gas phase) =
-2281.23141176
Zero-point correction= 0.505412
(Hartree/Particle)
Thermal correction to Energy =
0.539756
Thermal correction to Enthalpy =
0.540700
Thermal correction to Gibbs Free
Energy = 0.438249
SCF Energy (AcOH + D3) =
-2281.36030137
SCF Energy (PhMe + D3) =
-2281.34896433

2:ortho, (L:Me) PdCl₂

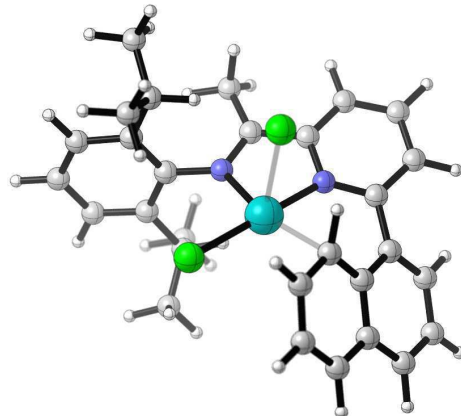
SCF Energy (gas phase) =
-1820.38825239
Zero-point correction= 0.492810
(Hartree/Particle)
Thermal correction to Energy =
0.524871
Thermal correction to Enthalpy =
0.525815
Thermal correction to Gibbs Free
Energy = 0.428620
SCF Energy (AcOH + D3) =
-1820.49625972
SCF Energy (PhMe + D3) =
-1820.48910619

2:peri, (L:Me) PdCl₂

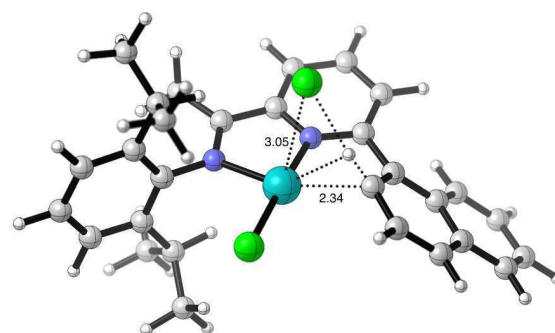
SCF Energy (gas phase) =
-1820.38380958
Zero-point correction= 0.492961
(Hartree/Particle)
Thermal correction to Energy =
0.524826
Thermal correction to Enthalpy =
0.525770
Thermal correction to Gibbs Free
Energy = 0.429626
SCF Energy (AcOH + D3) =
-1820.49536187
SCF Energy (PhMe + D3) =
-1820.48790615

TS (1a-A)

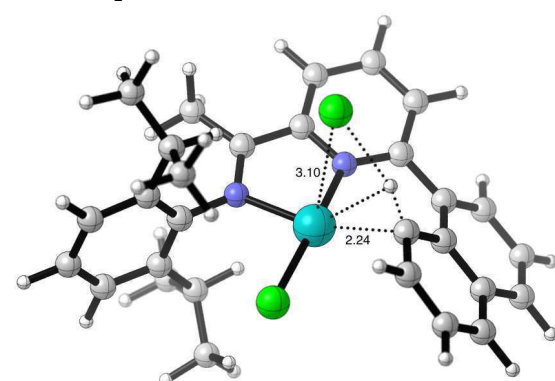
SCF Energy (gas phase) =
-2281.19599490
Zero-point correction= 0.504469
(Hartree/Particle)
Thermal correction to Energy =
0.538216
Thermal correction to Enthalpy =
0.539160
Thermal correction to Gibbs Free
Energy = 0.438966
Lowest frequency = -36.80cm⁻¹
SCF Energy (AcOH + D3) =
-2281.32581907
SCF Energy (PhMe + D3) =
-2281.31555391

A, (HL:Me)PdCl₂

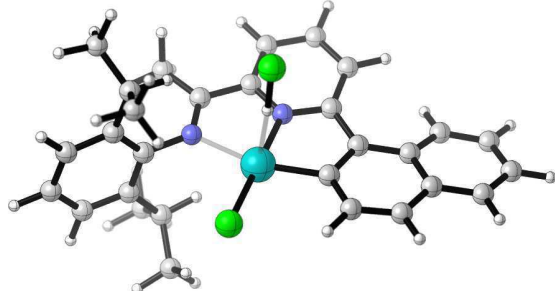
SCF Energy (gas phase) =
-2281.19916670
Zero-point correction= 0.504372
(Hartree/Particle)
Thermal correction to Energy =
0.538908
Thermal correction to Enthalpy =
0.539852
Thermal correction to Gibbs Free
Energy = 0.438454
SCF Energy (AcOH + D3) =
-2281.33556815
SCF Energy (PhMe + D3) =
-2281.32422110

TS (1a-B:ortho)

SCF Energy (gas phase) =
-2281.19138151
Zero-point correction= 0.502811
(Hartree/Particle)
Thermal correction to Energy =
0.536871
Thermal correction to Enthalpy =
0.537816
Thermal correction to Gibbs Free
Energy = 0.436125
Lowest frequency = -52.23cm⁻¹
SCF Energy (AcOH + D3) =
-2281.32686823
SCF Energy (PhMe + D3) =
-2281.31387283

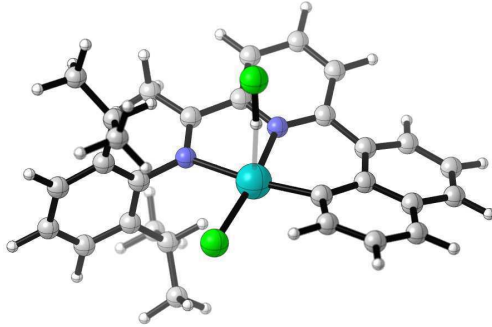
TS (A-B:peri)

SCF Energy (gas phase) =
-2281.19839780
Zero-point correction= 0.503726
(Hartree/Particle)
Thermal correction to Energy =
0.537422
Thermal correction to Enthalpy =
0.538367
Thermal correction to Gibbs Free
Energy = 0.439000
Lowest frequency = -29.77cm⁻¹
SCF Energy (AcOH + D3) =
-2281.33724852
SCF Energy (PhMe + D3) =
-2281.32496324

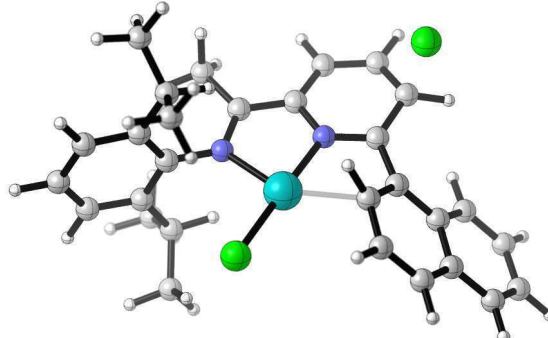
B:ortho, (L:Me)PdCl(HCl)

SCF Energy (gas phase) =
-2281.22434427

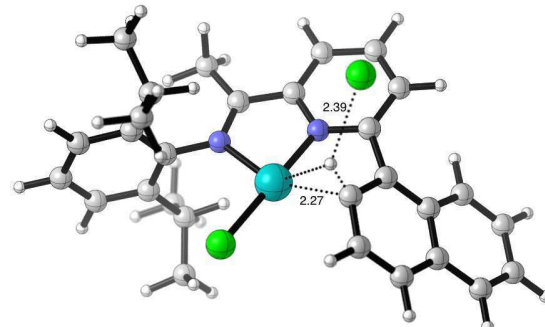
Zero-point correction= 0.500819
(Hartree/Particle)
Thermal correction to Energy =
0.535718
Thermal correction to Enthalpy =
0.536662
Thermal correction to Gibbs Free
Energy = 0.431977
SCF Energy (AcOH + D3) =
-2281.34490745
SCF Energy (PhMe + D3) =
-2281.33743048

B:peri, (L:Me)PdCl(HCl)

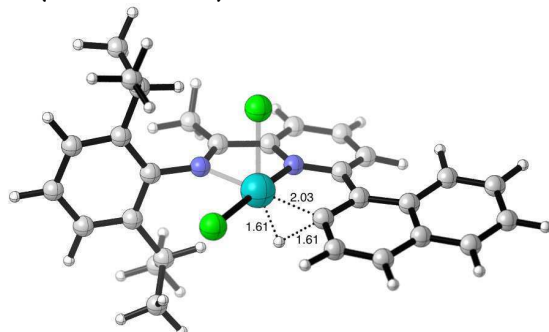
SCF Energy (gas phase) =
-2281.22103219
Zero-point correction= 0.501147
(Hartree/Particle)
Thermal correction to Energy =
0.535706
Thermal correction to Enthalpy =
0.536651
Thermal correction to Gibbs Free
Energy = 0.434295
SCF Energy (AcOH + D3) =
-2281.34530822
SCF Energy (PhMe + D3) =
-2281.33771636

C, [(HL:Me)PdCl] [Cl]

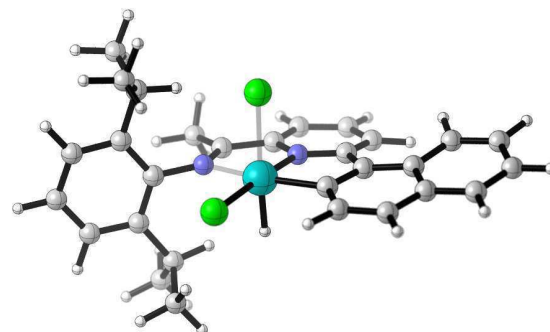
SCF Energy (gas phase) =
-2281.19117861
Zero-point correction= 0.504116
(Hartree/Particle)
Thermal correction to Energy =
0.538934
Thermal correction to Enthalpy =
0.539878
Thermal correction to Gibbs Free
Energy = 0.435827
SCF Energy (AcOH + D3) =
-2281.31349099
SCF Energy (PhMe + D3) =
-2281.30474228

TS(C-B:ortho)

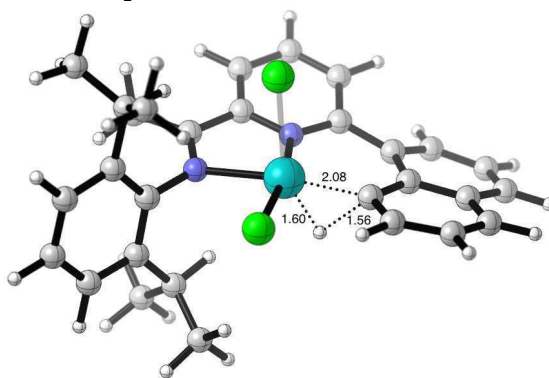
SCF Energy (gas phase) =
-2281.18540575
Zero-point correction= 0.503283
(Hartree/Particle)
Thermal correction to Energy =
0.537331
Thermal correction to Enthalpy =
0.538276
Thermal correction to Gibbs Free
Energy = 0.436493
Lowest frequency = -70.62cm⁻¹
SCF Energy (AcOH + D3) =
-2281.32196944
SCF Energy (PhMe + D3) =
-2281.30842954

TS (1a'-D:ortho)

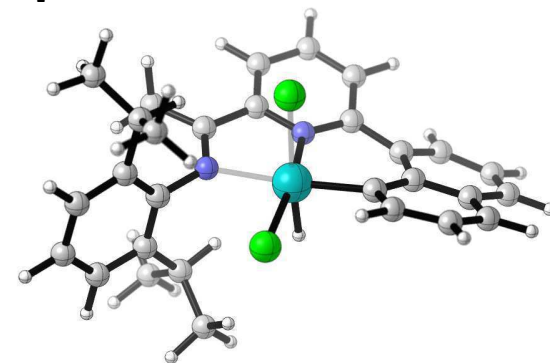
SCF Energy (gas phase) =
-2281.18153450
Zero-point correction= 0.500317
(Hartree/Particle)
Thermal correction to Energy =
0.534327
Thermal correction to Enthalpy =
0.535271
Thermal correction to Gibbs Free
Energy = 0.434625
Lowest frequency = -809.35cm⁻¹
SCF Energy (AcOH + D3) =
-2281.31017101
SCF Energy (PhMe + D3) =
-2281.29976042

D:ortho

SCF Energy (gas phase) =
-2281.19238414
Zero-point correction= 0.502370
(Hartree/Particle)
Thermal correction to Energy =
0.536546
Thermal correction to Enthalpy =
0.537491
Thermal correction to Gibbs Free
Energy = 0.436632
SCF Energy (AcOH + D3) =
-2281.32091185
SCF Energy (PhMe + D3) =
-2281.31093487

TS (1a-D:peri)

SCF Energy (gas phase) =
-2281.17488041
Zero-point correction= 0.500463
(Hartree/Particle)
Thermal correction to Energy =
0.534346
Thermal correction to Enthalpy =
0.535290
Thermal correction to Gibbs Free
Energy = 0.435641
Lowest frequency = -761.13cm⁻¹
SCF Energy (AcOH + D3) =
-2281.30754055
SCF Energy (PhMe + D3) =
-2281.29712525

D:peri

SCF Energy (gas phase) =
-2281.18903992
Zero-point correction= 0.502615
(Hartree/Particle)
Thermal correction to Energy =
0.536546
Thermal correction to Enthalpy =
0.537490
Thermal correction to Gibbs Free
Energy = 0.438274
SCF Energy (AcOH + D3) =
-2281.32084194
SCF Energy (PhMe + D3) =
-2281.31121408

HC1

SCF Energy (gas phase) =
-460.828400917
Zero-point correction= 0.006554
(Hartree/Particle)
Thermal correction to Energy =
0.008915
Thermal correction to Enthalpy =
0.009859
Thermal correction to Gibbs Free
Energy = -0.011345
SCF Energy (AcOH + D3) =
-460.83120917
SCF Energy (PhMe + D3) =
-460.83009372

References

- S1. Gaussian 09 (Revision E.01), M. J. Frisch, G. W. Trucks, H. B. Schlegel, G. E. Scuseria, M. A. Robb, J. R. Cheeseman, G. Scalmani, V. Barone, B. Mennucci, G. A. Petersson, H. Nakatsuji, M. Caricato, X. Li, H. P. Hratchian, A. F. Izmaylov, J. Bloino, G. Zheng, J. L. Sonnenberg, M. Hada, M. Ehara, K. Toyota, R. Fukuda, J. Hasegawa, M. Ishida, T. Nakajima, Y. Honda, O. Kitao, H. Nakai, T. Vreven, J. A. Montgomery, Jr., J. E. Peralta, F. Ogliaro, M. Bearpark, J. J. Heyd, E. Brothers, K. N. Kudin, V. N. Staroverov, T. Keith, R. Kobayashi, J. Normand, K. Raghavachari, A. Rendell, J. C. Burant, S. S. Iyengar, J. Tomasi, M. Cossi, N. Rega, J. M. Millam, M. Klene, J. E. Knox, J. B. Cross, V. Bakken, C. Adamo, J. Jaramillo, R. Gomperts, R. E. Stratmann, O. Yazyev, A. J. Austin, R. Cammi, C. Pomelli, J. W. Ochterski, R. L. Martin, K. Morokuma, V. G. Zakrzewski, G. A. Voth, P. Salvador, J. J. Dannenberg, S. Dapprich, A. D. Daniels, O. Farkas, J. B. Foresman, J. V. Ortiz, J. Cioslowski, and D. J. Fox, Gaussian, Inc., Wallingford CT, 2013.
- S2. (a) A.D. Becke, *Phys. Rev. A*, 1988, **38**, 3098; (b) J. P. Perdew, *Phys. Rev. B*, 1986, **33**, 8822-8824.
- S3. D. Andrae, U. Haeussermann, M. Dolg, H. Stoll, and H. Preuss, *Theor. Chem. Acc.*, 1990, **77**, 123-124.
- S4. (a) W. J. Hehre, R. Ditchfield, and J. A. Pople, *J. Chem. Phys.*, 1972, **56**, 2257; (b) P.C. Hariharan and J. A. Pople, *Theor. Chem. Acta*, 1973, **28**, 213-222.
- S5. S. Grimme, J. Antony, S. Ehrlich, and H. Krieg, *J. Chem. Phys.*, 2010, **132**, 154104.
- S6. J. Tomasi, B. Mennucci, and R. Cammi, *Chem. Rev.*, 2005, **105**, 2999-3093.
- S7. See references presented in the main text.